THE ROLE OF THE G PROTEIN-COUPLED RECEPTOR GPR62 IN REMYELINATION

by

Elizabeth Mary-Francys Davis Clawson

A dissertation submitted in partial fulfillment of

the requirements for the degree of

Doctor of Philosophy

(Molecular and Cellular Pharmacology)

at the

UNIVERSITY OF WISCONSIN-MADISON

2024

Date of final oral examination: May 8, 2024

The dissertation is approved by the following members of the Final Oral Committee:

Shing-Yan (Bill) Chiu, Professor, Neuroscience
Randolph S. Ashton, Associate Professor, Biomedical Engineering
Lara Collier, Associate Professor, Pharmaceutical Sciences
Jayshree Samanta, Assistant Professor, Comparative Biosciences (Advisor)

DEDICATION

This dissertation is dedicated to my family, who have been my biggest source of support throughout my lifetime educational journey. To my parents, Ron and Kathy Davis, for encouraging my nerdy science interests and always telling me I'm smarter and prettier than all the mean kids. To my six siblings Boo, Tini, Zuba, Jaime, Critter and Stuffy for cheering me on, reminding me to go write, sending pictures of their cute kids and fun vacations, and telling me I can actually do this. To my kids Mergle, Sam, and Ruby and my bonus kids, who have tolerated science lectures and weird dinner table conversations their whole lives. And most importantly, to my husband John, who is the biggest supporter and cheerleader of them all, I could not have done this without you and I wouldn't want to try.

ACKNOWLEDGEMENTS

While it's my name on the front page, the work in here would not have been done without the help of my labmates. Foremost, Jay for taking me into her lab, giving me a chance, pretending to laugh at my stupid jokes, and sharing all the best food spots (and all the cryosectioning, so much sectioning). To our intrepid lab manager Anna, for all her mouse breeding and genotyping, a huge thank you for all the PCR, especially the aggravating ones, but most of all the hugs. To my undergrad student Jordyn, who did so much cell counting she probably sees spots when she closes her eyes.

I would be remiss to not acknowledge the incredible supportive role of my grad student office crew, McKenna, Sharon and Bella. You may never know how much you and your friendship have meant to me and you will forever have a special place in my heart.

And the various lab members through the years who have taught me various skills and shared insights and late-night takeout, particularly Dan, Christian, and Sai who helped me learn a new field and get started in the lab, and Dev who helped with data analysis.

Finally a shoutout to the Yogo lab and the Emery lab for supplying the Gpr62 mouse lines used in this work.

ABSTRACT

Myelin formation during development and remyelination following injury is a tightly regulated process that is not well understood. The orphan G protein-coupled receptor Gpr62, which is enriched in mature myelinating oligodendrocytes, has previously been shown to be unnecessary in developmental myelination. Here, we show that Gpr62 is a regulator of process formation in remyelination by the Gli1-expressing neural stem cells from the subventricular zone of the adult mouse brain. Additionally, we demonstrate that Gpr62 signals through the cAMP pathway to downregulate oligodendrocyte maturation.

TABLE OF CONTENTS

LIST OF TABLES

LIST OF FIGURES

LIST OF ABBREVIATIONS

AA ..... Arachidonic Acid

AD ..... Alzheimer's Disease

cAMP ..... cyclic Adenine Monophosphate

CC ..... Corpus Callosum

ChIPseq ..... Chromatin Immunoprecipitation Sequencing

CNS ..... Central Nervous System

CREB ..... cAMP Response Element Binding Protein

DHA ..... Docosahexaenoic Acid

ECM ..... Extracellular Matrix

EVs ..... Extracellular Vesicles

FAs ..... Fatty Acids

FABP ..... Fatty Acid Binding Protein

GO ..... Gene Ontology

GPCR ..... G Protein-Coupled Receptor

KEGG ..... Kyoto Encyclopedia of Genes and Genomes

KO ..... Knockout

MBP ..... Myelin Basic Protein

MOG ..... Myelin Oligodendrocyte Glycoprotein

MS ..... Multiple Sclerosis

mTOR ..... Mammalian Target of Rapamycin

NSC ..... Neural Stem Cell

OL ..... Oligodendrocyte

OPC ..... Oligodendrocyte Progenitor Cell

PD ..... Parkinson's Disease

PI3K Phosphatidylinositol-3-Kinase

PKA ..... Protein Kinase A

PLP1 ..... Proteolipid Protein 1

PPMS ..... Primary Progressive Multiple Sclerosis

RRMS ..... Relapsing-Remitting Multiple Sclerosis

S1PR1 ..... Sphingosine-1-Phosphate Receptor 1

SPMS ..... Secondary Progressive Multiple Sclerosis

SVZ ..... Subventricular Zone

WT ..... Wild-type

CHAPTER ONE: INTRODUCTION

Myelin in the Central Nervous System

Myelin is one of the most important evolutionary developments in the vertebrate nervous system. Myelin sheaths are formed in the central nervous system (CNS)s by oligodendrocytes (OLs) (1). These glial cells extend a highly variable 10-60 processes to multiple neurons that wind around the axon to form tight, compact layers (2). The myelin sheath insulates the axon and allows efficient signal propagation by saltatory conduction, resulting in a dramatic increase in the nerve conduction velocity. This is facilitated by the nodes of Ranvier; spaces in between the myelin wrapped areas that contain a higher concentration of ion channels in the axon than in the internodes (3).

As the OL process extends around the axon circumference, it also expands longitudinally to increase the length of the myelin internode, the lengths of which range between 20-200 μm (2). The OL processes creating the myelin layers are compacted until almost all the cytosol is extruded from the process. These layers are comprised mainly of lipids (70-80%) (4), including phospholipids, galactolipids, and cholesterols, the ratios of which change during development and maturation (5). These lipids are built from Fatty Acids (FAs), the hydrophobicity of which requires protein transporters to carry them through the aqueous cytosol. One group of these transporters is a family of 12 proteins-

called Fatty Acid Binding Proteins (FABPs), of which three (FABP3, FABP5, and FABP7) are found in the CNS (6). Of these, FABP7 has been linked to oligodendrocyte differentiation (7).

Myelin in Disease

In addition to the role of myelin in increasing the speed of the action potential down the axon, OLs provide metabolic support to the axons, which can be quite long and therefore far from the neuronal cell body Myelinated neurons can become dependent on OLs, as evidenced by axonal degeneration and neuronal death following the loss of OLs, thus demonstrating the critical nature of this support (8, 9). Not surprisingly, many neurodegenerative diseases have comorbid demyelination. Well-known examples of these include Alzheimer's disease (AD) and Parkinson's disease (PD). While not well understood, AD and PD are primarily characterized biologically by protein dysregulation (amyloid-β & tau and α-synuclein, respectively) (10, 11) leading to neuronal cell death and demyelination which manifests clinically as dementia and motor control deficits. In contrast, Multiple Sclerosis (MS) is an autoimmune demyelinating disease of the CNS, the lesions of which can be seen in diagnostic imaging and post-mortem histology The most common form of MS is the relapsing-remitting form (RRMS), where patients have periods of myelin loss (relapse) alternating with periods of remyelination (remission). This can continue for decades and eventually progress to secondary progressive MS (SPMS), where the disease grows progressively worse with little or no recovery. The most severe form of

MS, primary progressive (PPMS), is characterized by persistent deterioration of myelination with little or no recovery from onset (12, 13). Particularly in MS, finding solutions to regenerate myelin following a demyelinating event will present a giant leap forward in therapeutic treatment. Currently, none of the drugs available to treat neurodegenerative diseases promote remyelination, they only function to curb further progression of the disease.

If the damaged myelin can be regenerated in a timely manner, axonal degeneration can be prevented and neuronal function can be restored (14). Oligodendrocytes (OLs) originally develop from neural stem cells (NSCs) via different stages of differentiation marked by the expression of specific markers i.e., NSCs develop into oligodendrocyte progenitor cells (OPCs) which differentiate into OLs, which then mature into myelinating OLs (15-18). Following injury in the adult brain, myelin can be regenerated by three sources. First, if the existing oligodendrocytes in the injury area are still viable, they have a limited ability to re-establish their axonal association (19, 20), however, this pathway for myelin regeneration is not particularly efficient or accurate (21, 22). Second, OPCs residing throughout the adult brain can activate and differentiate into OLs to remyelinate the neurons in their vicinity (23). Finally, the third source of myelin regeneration is the NSCs themselves (24, 25).

Cell Populations Contributing to Myelin Regeneration

Mature Oligodendrocytes

Until recently, the contribution of mature oligodendrocytes to remyelination was considered negligible, if at all (26, 27). It has now been demonstrated that mature oligodendrocytes are able to participate in remyelination, however, the myelin formed by these cells has shorter internodes, thinner sheaths, and is often found to be mistargeted to neuronal cell bodies (19-22, 28). A recent study also suggested that mature oligodendrocytes play a major role in remyelination in the brains of people with MS (20, 29). This lower efficiency and accuracy in remyelination by mature oligodendrocytes could partially explain the lower rates of remyelination in humans compared to mouse models.

Oligodendrocyte Progenitor Cells

A ubiquitous population of oligodendrocyte progenitor cells (OPCs) reside throughout the CNS. In response to a demyelinating insult OPCs rapidly mobilize and migrate to the lesions in their vicinity (23). These OPCs then differentiate and mature into myelinating OLs for remyelinating surviving axons (29). They do so in an efficient and accurate manner, though these myelin sheaths tend to be thinner and have shorter internodes than the original myelin (30). This mechanism is recognized as the primary pathway for regenerating myelin in the CNS.

Neural Stem Cells in the Subventricular Zone

NSCs residing in the subventricular zone (SVZ), lining the walls of the lateral ventricles in the adult brain, can differentiate into astrocytes, neurons, and oligodendrocytes *in vitro* (17, 18). Our lab has demonstrated that a subpopulation of NSCs in the ventral SVZ that express the transcription factor Gli1, migrate to sites of demyelinating injury in the white matter corpus callosum (CC) (24). In a healthy brain, these cells preferentially migrate to the olfactory bulb and differentiate into neurons and astrocytes. However, when activated following a demyelinating injury, these Gli1 NSCs instead migrate to the CC and differentiate into OPCs and myelinating OLs. This recruitment and differentiation into OLs is further enhanced when Gli1 is inhibited genetically or pharmacologically (24). Thus, $Gli1^{Null}$ mice have a higher capacity for myelin repair compared to Gli1-expressing $Gli1^{Het}$ mice (24).

We performed an RNA-seq on NSCs harvested from $Gli1^{Het}$ and $Gli1^{Null}$ mice and found the expression of the orphan GPCR Gpr62 to be significantly reduced in the $Gli1^{Het}$ NSCs compared to $Gli1^{Null}$ NSCs following demyelination, suggesting a role for Gpr62 in remyelination (31) (NCBI Geo GSE162683). Interestingly, autoantibodies against Gpr62 have been found in blood samples from MS patients (32) and are also shown to be upregulated in the more aggressive primary progressive form of MS compared to RRMS (33), suggesting that autoimmune-mediated loss of Gpr62 may either play a role in the loss of OLs or have an effect on myelin regeneration.

GPCRs in Myelin Regulation

Results from several studies indicate that Gpr62 is expressed in mature oligodendrocytes and may have a role in regulating oligodendrocyte maturation. A transcriptomic study of gene expression in the different cells of the neonatal brain showed that Gpr62 mRNA expression increases with maturation of the oligodendroglial cells, with the highest expression in myelinating oligodendrocytes, suggesting that Gpr62 may regulate oligodendrocyte maturation (34, 35). Allen Brain Atlas shows Gpr62 to be 12-fold more highly expressed in telencephalic white matter, which is enriched with myelinating OLs compared to the cortex, consistent with genetic ablation of OLs in the mouse brain (36, 37). CHIPseq data from several labs further indicate that the Gpr62 promoter contains binding sites for transcription factors Olig2 and MyrF, essential for oligodendrogenesis, suggesting a direct regulation of Gpr62 during OL differentiation (38, 39).

Gpr62 is a G protein-coupled receptor (GPCR), which is the largest group of transmembrane proteins. They represent an extremely diverse group of receptors, and their ligands span a large variety of factors, including protein ligands, hormones, small molecules, organic compounds, and even light. They are grouped into five phylogenetic families based on homology and functional similarity. They include the Glutamate, Rhodopsin, Adhesion, Frizzled, and Secretin families, with the Rhodopsin family being the largest. Gpr62 is classified as a Class A Rhodopsin-type GPCR., which also includes many GPCRs involved in neurotransmission and neurogenesis critical for taste, smell, and vision (40, 41). GPCRs are characterized by their seven membrane-spanning domains and their activation of the various intracellular heteromeric guanine nucleotide-binding protein (G

protein) complexes. These complexes are made up of a $G_{\beta\gamma}$ dimeric complex and a G_{α} subunit. G_{α} subunits have a variety of subtypes, four key types being $G_{\alpha s}$, $G_{\alpha q}$, $G_{\alpha i/o}$, and $G_{12/13}$. Gpr62 has been shown to signal through both $G_{\alpha s}$ and $G_{\alpha q}$ subunit types, but not through $G_{\alpha i/o}$ (42). However, the role of Gpr62 in remyelination remains unknown. A summary of OL development-associated GPCRs is given in Table 1.

Table 1. GPCRs involved in oligodendrocyte development

GPCR	Family	Glial cell expression	Ligand in glia	G-protein signaling	Reference
Cxcr4	Rhodopsin	OPC, astrocyte	Cxcl12	$G\alpha_i$	(43, 44)
EDNRB	Rhodopsin	OPC, astrocyte	endothelin	$G\alpha_q$	(45, 46)
Gpr17	Rhodopsin	OPC, new OL	unknown	$G\alpha_{i/o}$	(47, 48)
Gpr30	Rhodopsin	OPC, new OL	estrogen	$G\alpha_s$, $G\alpha_{i/o}$	(49-51)
Gpr37	Rhodopsin	new OL, mature OL	unknown	$G\alpha_s$	(52)
Gpr56	Adhesion	OPC, astrocyte	collagen III	$G\alpha_{12/13}$	(53, 54)
Gpr62	Rhodopsin	new OL, mature OL	C1q (*in vitro* only)	$G\alpha_s$, $G\alpha_q$	(55)
Gpr98	Adhesion	OPC, neuron, astrocyte	unknown	$G\alpha_{i/o}$	(56)
κ-opiod	Rhodopsin	neuron, astrocyte, mature OL	dynorphin-B	$G\alpha_{i/o}$	(57)
mGlu4	Glutamate	OPC, new OL, neuron	glutamate	$G\alpha_{i/o}$	(58, 59)
S1PR1	Rhodopsin	OPC, astrocyte	lipids	$G\alpha_{i/o}$	(60)

Several studies have identified the functions of different GPCRs in myelination. Among these, there are two GPCRs from the rhodopsin family that have a similar

expression pattern in the oligodendroglial lineage as Gpr62 e.g., sphingosine-1-phosphate receptor 1 (S1PR1) and Gpr37 (34, 52, 61). However, unlike Gpr62 which constitutively activates cyclic adenine monophosphate (cAMP) (42, 62), both S1PR1 and Gpr37 inhibit cAMP activity. Both GPCRs are also negative regulators of myelination. cAMP is the most common downstream second messenger of G protein signaling involved in many biological processes, including adult oligodendrogenesis and differentiation (63, 64). It is generated by $G_{\alpha s}$ protein-activated adenylyl cyclase (AC) and signals through a variety of downstream effectors. The GPCR/AC/cAMP pipeline is activated in response to various elements, including adhesion to a surface which activates a myelinogenic environment, as well as ligand binding to GPCRs (65). The most prolific and best-characterized cAMP downstream effector is Protein Kinase A (PKA), which in turn activates a plethora of transcription factors, including the cAMP response element binding protein (CREB). CREB is also activated by Protein Kinase C (PKC). CREB and cAMP appear to have differing effects on oligodendrocyte development and differentiation depending on the stage of the differentiation progression. In early differentiation, PKA activation of CREB mediates the transition from OPCs to immature OLs, while later PKC activation of CREB mediates immature OLs advancing to mature OLs (64, 66). CREB has been demonstrated to activate myelin-associated genes, including myelin basic protein (MBP), 2',3'-cyclic nucleotide 3'-phosphodiesterase (CNPase), proteolipid protein (PLP), and myelin oligodendrocyte glycoprotein (MOG) (67-70). Fittingly, cAMP analogs have a protective effect on myelin and decrease the apoptosis of oligodendrocytes (71, 72). cAMP inhibits OPC proliferation, but once the cells have committed to OL differentiation, cAMP

independently stimulates OL differentiation (68, 73, 74). In contrast, cAMP inhibits the phosphorylation of MBP, which is needed for MBP localization in the myelin sheath and in immortalized cell culture. Indeed, cAMP induction upregulates PLP expression while cAMP analogs down-regulate MBP gene expression (75-77). By contrast, PKC phosphorylates MBP and promotes MBP synthesis (78). The role of primary cilia in OL differentiation is an understudied question, but recently these specialized compartments have been implicated in regulating CREB developmental proliferation, as well as in response to demyelination (79).

It is currently unknown which specific GPCRs are involved upstream of cAMP that regulate oligodendrogenesis and remyelination. Gpr62 has been shown to constitutively activate cAMP, with a dosage-dependent effect i.e. increasing cAMP activity with increasing Gpr62 levels (42). This would suggest Gpr62 as a potential upstream partner in cAMP signaling and, when combined with the data from other studies (31), a possible key player in cAMP signaling in oligodendrogenesis and remyelination, given its increased expression as OLs differentiate and mature.

In addition to cAMP, GPCRs also signal via recruitment of β-arrestin (reviewed in (80, 81)). β-arrestin can signal both through G protein-mediated pathways, and independently. It serves as a scaffold for the assembly of various kinases, which frequently trigger the MAP/ERK signaling pathway. One of the GPCRs involved in demyelination, Gpr17, signals through β-arrestin (82) and ERK1/2 (47), as well as the $G_{\alpha i/o}$ signaling pathway to reduce cAMP activity resulting in apoptosis (48). While Gpr62 is also capable

of recruiting and internalizing β-arrestin constitutively (42), the functional significance of signaling via cAMP vs β-arrestin recruitment is not known.

Another pathway downstream of GPCRs is the PI3K/Akt/mTOR pathway. Mammalian Target of Rapamycin (mTOR) is involved in regulating many cellular pathways, including those involved in protein synthesis, cell growth, and of particular interest to our lab, myelination. mTOR has different roles at different points along the differentiation and maturation timeline, from developmental myelination to remyelination. During myelination, mTOR signaling is downstream of ERK1/2 and PI3K-Akt pathways, and the two pathways working synergistically. Some of the myelination processes mTOR is implicated in include; the transition from OPC to OL (83-86), directing axon wrapping (87), maintaining myelin integrity (88), and mobilizing existing OLs for remyelination (89, 90). Additionally, mTOR is involved in initiating myelination and regulating cytoskeletal modulation (87, 91), OL process branching complexity (91), timely onset of remyelination (90, 91), promoting OL differentiation and maturation (84, 90, 92), appropriate wrapping to the axon diameter (86, 88, 93), and extent of myelination (94, 95). Throughout these studies, mTOR has repeatedly been excluded as a regulator of OPC proliferation.

There are more than 700 GPCRs, and more than 100 of them have unknown ligands, also known as “orphan GPCRs”. As GPCRs are cell-surface receptors, they are of great interest in the pharmacology field due to their potential druggability. Approximately 30-40% of drugs on the market target GPCRs, so orphan GPCRs offer potentially new drug targets in a myriad of diseases. While a previous study found that the innate immune component C1q can bind to Gpr62 *in vitro*, the study did not go as far as investigating any

effect C1q-Gpr62 binding has on downstream signaling (55). Thus, Gpr62 arguably falls into the category of orphan GPCR, as its endogenous ligands have yet to be identified.

Fatty Acid Binding Proteins in Oligodendrocytes

Myelin is highly enriched with lipids. Lipids give myelin its insulating properties and based on the specific composition of fatty acids, allow for region-specific control of membrane stiffness. Galactolipids and phospholipids are the two main lipids found in myelin and are built from fatty acids (4). OL fatty acid synthesis and transport are essential for myelination and remyelination in the CNS (96). Given their highly hydrophobic nature, fatty acids require a chaperone to transit the water-based cytoplasm. Fatty Acid Binding Proteins (FABPs) fill this role. Of the 10 members of the FABP family, three, FABP3, FABP5, and FABP7, are found in the CNS.

Two long-chain fatty acids in particular, Docosahexaenoic Acid (DHA) and Arachidonic Acid (AA), are highly enriched in the brain, and the DHA:AA ratio is important to maintain brain health (97, 98). DHA and AA are the primary omega-3 and omega-6 fatty acids in the brain, respectively. Both of these fatty acids are bound by Fabp7 and Fabp7 uptake of DHA has been shown in glioblastoma neural-like stem cells (98). DHA in particular has been suggested to promote differentiation of oligodendrocytes and is necessary for fatty acid synthesis in OLs (96, 99). When Fabp7 is knocked down in neonate-derived cultured OPCs, the cells do not differentiate into mature OLs (7). The importance of fatty acid transport in myelination can be seen in studies of diseases

involving mutations in FA transporters, for example a DHA transporter. Diseases caused by partial or full inactivation of a DHA transporter, sodium-dependent lysophosphatidylcholine transporter, or major facilitator superfamily domain-containing protein 2 (MFSD2A) resulted in hypomyelination, microcephaly, and decreased white matter volume (100-102).

The rising expression of Gpr62 as OLs differentiate and mature suggests an important role for Gpr62 in myelin regulation. While previous studies have shown Gpr62 to be dispensable to fertility as well as developmental myelination (62, 103), none have looked at the role of Gpr62 in remyelination from adult neural stem cells. Here we demonstrate that Gpr62 inhibits OL maturation and that this effect is mediated via cAMP.

CHAPTER TWO: GPR62 IS ASSOCIATED WITH OLIGODENDROCYTE MATURATION

Gpr62 is expressed in neural stem cells and myelinating oligodendrocytes

Based on the results of our RNA-seq analysis of $Gli1^{HET}$ mice vs. $Gli1^{NULL}$ mice during demyelination which showed a decreased expression of Gpr62 in $Gli1^{HET}$ mice during demyelination but no decrease in $Gli1^{NULL}$ mice which show enhanced remyelination (Figure 1a), we wanted to confirm that Gpr62 expression is higher in myelinated tissue. To do this, we examined Gpr62 gene expression in healthy brain tissue compared to demyelinated brain tissue. To induce demyelination, we used the cuprizone model of demyelination and remyelination. Cuprizone, a copper chelator, has been used for more than 50 years as a model of demyelination and remyelination in multiple sclerosis studies in the rodent brain (104). When ingested by mice, cuprizone induces the death of oligodendrocytes, particularly in the corpus callosum. Depending on how long the mice are on the cuprizone diet, the demyelinated regions may spontaneously remyelinate. Acute demyelination results from 5-10 weeks of cuprizone diet with peak demyelination occurring at five weeks, and spontaneous remyelination occurring upon cessation of cuprizone. However, if chronic demyelination is induced with a longer period of ingestion (10+ weeks), the lesions do not remyelinate (105, 106).

We fed 8-12 week old WT mice a diet of either 0.2% cuprizone or regular chow as a control, for five weeks to achieve peak demyelination. The mice were then euthanized

and their brains collected. We extracted the mRNA from the corpus callosum and analyzed Gpr62 transcription by qPCR. These results showed a 75% decrease in Gpr62 gene

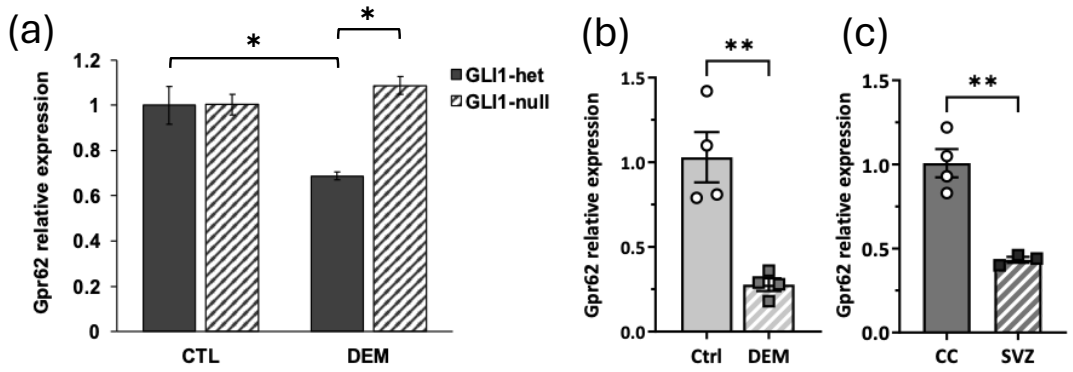

Figure 1. Gpr62 is highly expressed in myelin-rich brain regions.

(a.) Relative expression of Gpr62 in $Gli1^{HET}$ and $Gli1^{NULL}$, healthy vs. demyelinated brains. (Two-way ANOVA with Tukey's post hoc test; n=3), (b.) RT-qPCR from WT healthy (Ctrl) and demyelinated (DEM) mouse brain tissue. (Unpaired t test; n=4), (c.) RT-qPCR from healthy mouse central nervous system (CNS) subventricular zone (SVZ) and corpus callosum (CC). (Unpaired t-test; CC: n=4; SVZ: n=3), Error bars = SEM, *p<0.05, **p<0.01, ***p<0.001

expression in the demyelinated tissue compared to the healthy control (-0.7525 ± 0.1526) (Figure 1b). This suggests that Gpr62 expression was lost when myelinating oligodendrocytes died.

To further confirm that Gpr62 is higher in myelinating cells compared to neural stem cells, we examined the expression of Gpr62 in two distinct regions of the healthy adult mouse brain; the subventricular zone (SVZ) where the adult neural stem cells reside, and the corpus callosum, which is enriched with myelinating oligodendrocytes. We collected the brains from four 8-12 week old WT male and female mice and dissected the corpus callosum and SVZ. After extracting and purifying the mRNA, we performed qPCR

to analyze Gpr62 gene expression. We found a ~50% reduction of Gpr62 expression in the SVZ where neural stem cells reside compared to the corpus callosum-containing myelinating oligodendrocytes (-0.5742 ± 0.1004) (Figure 1c). This suggests that Gpr62 is expressed in NSCs but has a higher expression in an area of the brain with a greater density of myelinating oligodendrocytes.

Together these results suggest that Gpr62 is most highly expressed in myelinated oligodendrocytes. This is consistent with previous research which showed Gpr62 expression is highest in mature myelinating oligodendrocytes compared to immature oligodendrocytes and oligodendrocyte progenitor cells (34, 35, 103). Prior research has also shown that Gpr62 is expressed in human NSCs and OLs (55).

Genetic loss of Gpr62 increases OL maturation *in vitro*.

We then wanted to examine whether Gpr62 is necessary for differentiation of adult neural stem cells (NSCs) from the SVZ into the oligodendroglial lineage. In healthy brains, Gli1-expressing neural stem cells from the SVZ preferentially migrate through the rostral migratory stream to the olfactory bulbs and differentiate into interneurons and astrocytes (18, 107). In a healthy brain, they do not become oligodendrocytes. As previously reported by our lab (24), in response to a demyelinating injury, this same cell population is recruited to the site of injury, particularly in the corpus callosum, and differentiate into oligodendrocytes and astrocytes *in vivo* However, these NSCs are multipotent stem cells and have the potential to differentiate into the three lineages *in vitro*; neuron, astrocyte, and

oligodendrocyte. We obtained the global Gpr62 knockout mice (Gpr62-KO) generated by the Yogo Lab at Shizuoka University, Japan, and described in Muroi, et. al., 2017 (62). We harvested NSCs from the SVZs of three 8-12-week-old adult WT and three Gpr62-KO mice. We grew the NSCs as neurospheres in proliferation media, passaging three times before plating them on matrigel-coated coverslips with differentiation media. Under these conditions, we differentiated the NSCs for 14 days (Figure 2a). Using our protocol, we have previously demonstrated that this timeframe is sufficient for NSCs to differentiate into myelin producing oligodendrocytes (PLP+) as well as OPCs (NG2+), astrocytes (GFAP+), and neurons (Tuj1+) (108). We found the NSCs of Gpr62-KO mice differentiate into the three lineages, similar to WT NSCs (Figure 2b). However, there was a significant increase in the number of OPCs in the KO compared to the WT NSCs (WT: 8.68% +/- 1.73; KO: 19.20 +/-2.56) (Figure 2c). The proportion of neurons, astrocytes, and mature OLs were similar in the Gpr62-KO and WT NSCs.

Although the number of OLs did not change in the Gpr62-KO NSC cultures, we noticed some striking morphological differences in the OLs generated from Gpr62-KO NSCs (Figure 2b, OL panels). Primarily among them was an increase in process branching in the Gpr62-KO OLs. Since higher-order branching is a characteristic of more mature oligodendrocytes, this suggested that loss of Gpr62 increases the maturation of OLs (109). To quantify the extent of the process branching, we performed Scholl analysis which is commonly used to characterize neuron arborization and can be readily adapted to oligodendrocyte process branching (110). It involves overlaying concentric circles starting

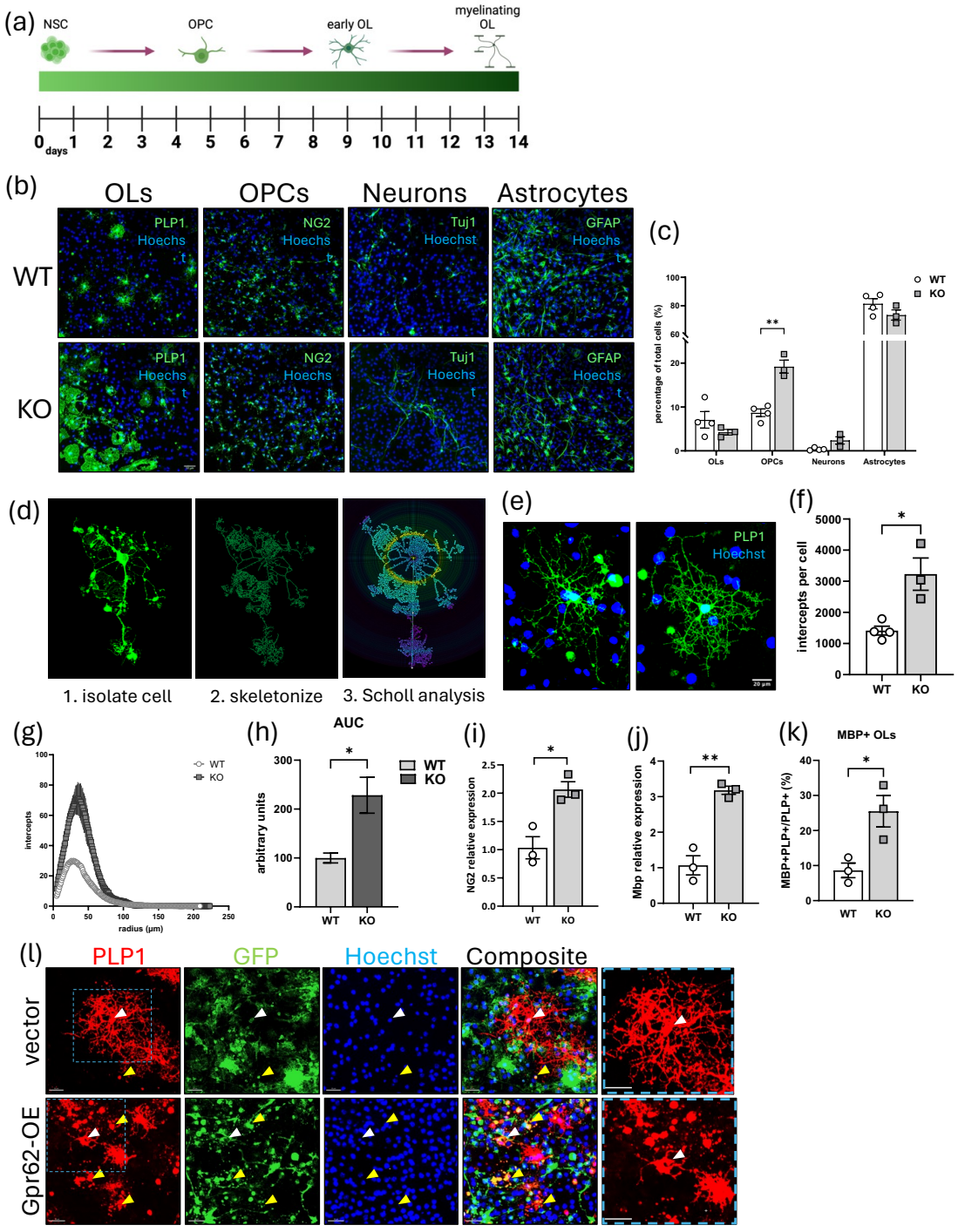

Figure 2. Global loss of Gpr62 increases maturation of oligodendrocytes *in vitro*.
(a.) Cell culture experimental timeline. (b.) Representative images of NSCs harvested from WT and KO mice and differentiated in vitro for 14 days. (Scale bar = 50 µm) (c.) Quantification of cell

types from in vitro 14-day differentiation. (Two-way ANOVA with Tukey's post hoc test; WT n=4, KO: n=3) (d.) NG2 expression in NSCs harvested from WT and KO mice and differentiated in vitro for 14 days. (e.) MBP expression in NSCs harvested from WT and KO mice and differentiated in vitro for 14 days. (f.) Percentage of MBP+PLP+ cells in the PLP+ population from NSCs harvested from WT and KO mice and differentiated for 14 days. (g.) Scholl analysis workflow. (h.) Representative images of WT and Gpr62-KO oligodendrocytes. scale bar = 20 μm (i.) Quantification of intercepts per cell. (Unpaired T-test; WT: n=4; KO: n=3) (j.) Average intercepts at each radius from Scholl analysis. (k.) Area under the curve (AUC) of (j.). (l.) Representative images of NSCs harvested from WT mice infected with Gpr62 OE virus and differentiated in vitro for 14 days. (White arrowhead: virus-infected PLP+ OL; Yellow arrowhead: remnants of dead or dying virus-infected cells; Scale bar = 30 μm), WT = wildtype; KO = Gpr62 global knockout; OE = overexpression; error bars = SEM, *p<0.05, **p<0.01, ***p<0.001

around the cell body and radiating out at regular intervals and counting when the circles intercept a cell process (111) (Figure 2d).We isolated images of single PLP+ oligodendrocytes and used a 5 μm start radius around the cell soma with 1 μm intervals between the concentric radii. We found that the Gpr62-KO NSC-derived OLs had significantly more process branching than WT cells, demonstrated by a higher number of total intercepts per cell (WT: 1413 +/-282.4; KO: 3230 +/-899.2) (Figure 2e, 2f). Figure 2g, 2h shows the intercepts per radius of the WT vs. Gpr62-KO cells. These results suggest a role for Gpr62 in regulating oligodendrocyte process branching.

We theorized that a more mature morphology would also be reflected in the gene expression. We collected neural stem cells from 8-12-week-old adult WT and Gpr62-KO mice, grew them as neurospheres with proliferation growth factors, followed by plating on Matrigel-coated coverslips for differentiation. These cells were collected after 14 days of differentiation and the mRNA was analyzed with qPCR analysis. We found that expression of the OPC marker NG2 was increased two-fold in the Gpr62-KO OLs compared to WT OLs (1.997 +/-0.216 fold change) (Figure 2i). Additionally, we found a three-fold increase

in the expression of the myelin protein MBP, which is only found in mature, myelinating oligodendrocytes, in the Gpr62-KO cells (2.974 +/-0.115 fold change) (Figure 2j). These results suggest that loss of Gpr62 in neural stem cells leads to an increase in oligodendrocyte maturation.

Myelin proteins are expressed in oligodendrocytes in a particular order, starting with PLP followed by MBP, MAG, and MOG (112). To gauge whether the PLP+ Gpr62-KO NSC-derived OLs are more mature than those from WT NSCs after 14 days of differentiation, we counted the number of PLP+ OLs that co-expressed MBP. We found a significant increase in the proportion of PLP+ cells that co-expressed MBP (+16.9% +/-5.28%) in the Gpr62-KO group (Figure 2k). This suggests that OLs generated from Gpr62-KO NSCs are more mature at 14 days of differentiation compared to WT OLs. Together these results suggest that Gpr62 inhibits or delays the maturation of oligodendrocytes.

To confirm the effect of Gpr62 on OL process branching, we developed a Gpr62 overexpression lentivirus (pLV-Gpr62-eGFP) and infected neural stem cells with the virus or vector on the first day of differentiation. After 14 days of differentiation, we found some striking changes in the cell morphology. We found very few OLs at all in the Gpr62-overexpressing population, and those few cells that were expressing PLP had few processes with little to no branching compared to the vector-infected OLs (Figure 2l.). This suggests that Gpr62 plays a role in restricting process growth and branching of OLs.

CHAPTER THREE: GPR62 REGULATES REMYELINATION

Gpr62 does not protect against demyelination

We considered the potential for an effect on the survival of OLs during demyelination. We used the cuprizone model of demyelination on 8-12-week-old adult WT and Gpr62-KO mice. We fed three male and three female WT and Gpr62-KO mice a diet of either 0.2% cuprizone or regular chow for five weeks. At the end of five weeks, the mice were euthanized and the harvested brains were cryosectioned for immunofluorescent labeling with PLP to evaluate the extent of demyelination in the corpus callosum (CC) (Figure 3a). While the cuprizone treatment resulted in significant decreases in myelin in both WT (WT REG: 93.31% +/-1.56% WT CUP: 31.02% +/-2.53%) and KO (KO REG 91.59% +/-1.94%; KO CUP: 28.83% +/-3.57) corpus callosum, we found no significant difference between WT and the KO mice (Figure 3b, 3c). This suggests that Gpr62 does not confer a protective element against cuprizone-mediated demyelination and demonstrates that cuprizone is comparably effective in both WT and KO mice.

Loss of Gpr62 increases myelinating oligodendrocytes in the corpus callosum

After eliminating a protective role for Gpr62 in demyelination, we turned toward viewing its potential effect on remyelination from the Gli1+ quiescent NSCs residing in the SVZ of the adult mouse brain. Our previous research has demonstrated that these NSCs are recruited to the corpus callosum for remyelination following acute demyelination in the

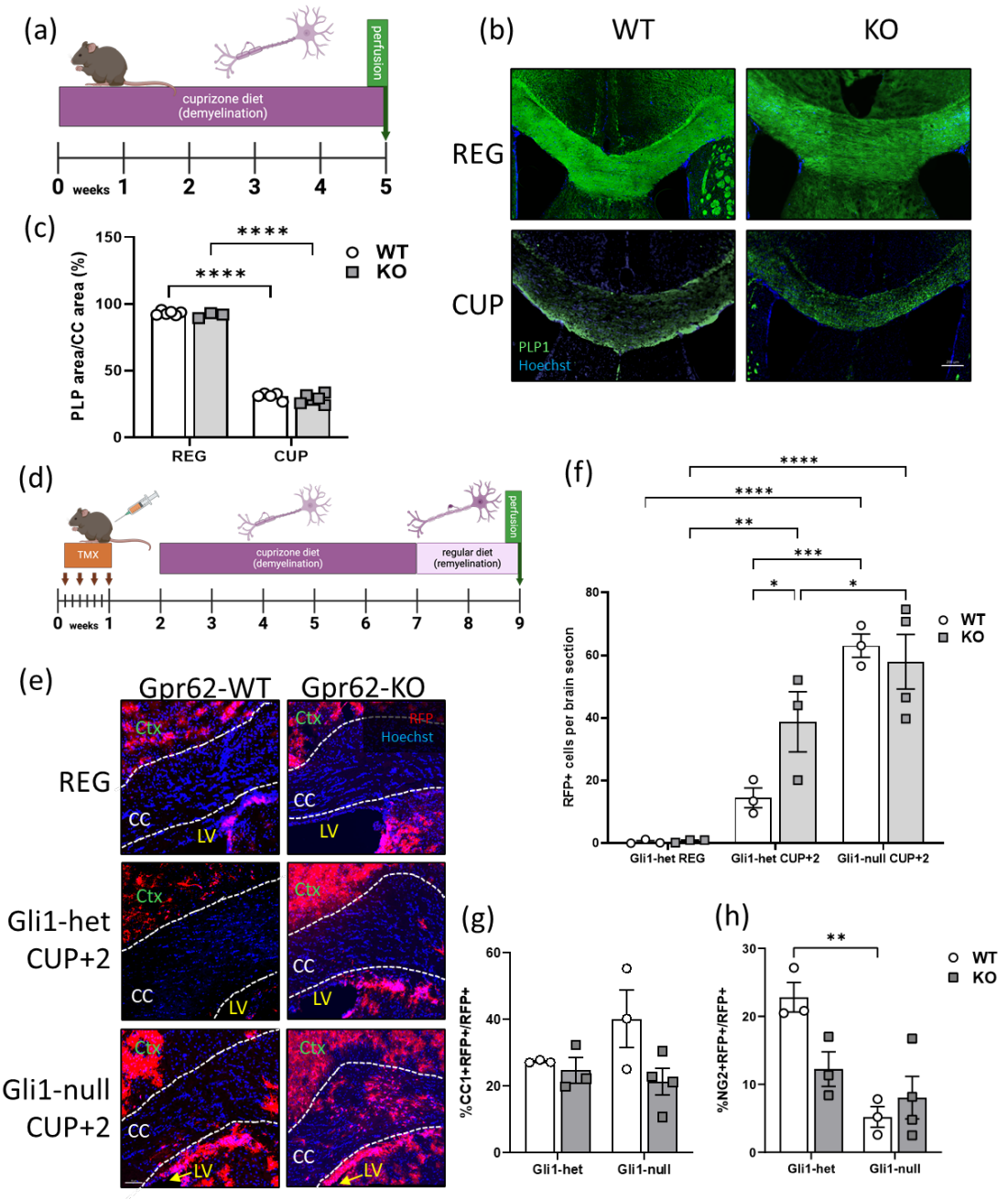

Figure 3. Global loss of Gpr62 does not protect against demyelination.

(a.) Timeline of demyelination experiment. (b.) Representative images of WT or KO mouse CC after 5 weeks of 0.02% cuprizone diet (CUP) or regular diet (REG). (scale bar = 200 um) (c.) quantification of (a.); percentage of myelin in corpus callosum after five weeks demyelination. (Two-way ANOVA with Tukey's post hoc test WT REG: n=6; KO REG: n=3; CUP WT: n=5; CUP KO: n=6) (d.) Timeline for remyelination experiment. (e.) Representative images for WT or

KO, Gli1-het and Gli1-null CC after regular diet (REG) or five weeks of 0.02% cuprizone diet followed by two weeks of regular diet (CUP+2) (Scale bar = 50 μm) (f.) Quantification of (e.) (Two-way ANOVA with Tukey's post hoc test; n=3 for all but KO CUP+2: n=4) (g.) Representative image of CC1+RFP+ and NG2+RFP+ cells in remyelinated CC. (Scale bar = 20 μm) (h.) Percentage of remyelinating cells differentiated into mature OLs and OPCs. (Unpaired t-tests on individual cell types) WT = wildtype; KO = Gpr62 global knockout; CC = corpus callosum; Ctx = cortex; LV = lateral ventricle, Error bars=SEM, *p<0.05, **p<0.01, ***p<0.001, ****p<0.0001

adult mouse brain (24). To track the NSCs that respond to demyelination, we crossbred the Gpr62-KO mouse line with our Gli1-fate mapped mouse line, *Gli1*^{CreERT};*Ai9*^{FX} to generate Gli1^{CreER};Gpr62^{KO}; Ai9 mice. In these mice, the Gli1-expressing cells in the SVZ, and all the daughter cells generated from them, express tdTomato for the lifetime of the cell following tamoxifen administration. By subjecting these mice to tamoxifen treatment before acute cuprizone-mediated demyelination, we can trace the lineage of the Tdtomato (RFP+) cells derived from the Gli1 expressing NSCs in the demyelinated injury site, even after they have differentiated into various cell types and have lost their Gli1 expression. Additionally, we can use immunofluorescent staining to determine which cells they differentiate into. We injected four, eight-week-old, *Gli1*$^{CreER/+}$;*Gpr6*$^{-/-}$*Ai9* (Gli1^{HET};Gpr62^{KO}) and *Gli1*$^{CreER/+}$;*Ai9* (Gli1^{HET};Gpr62^{WT}) mice with tamoxifen to permanently label the NSCs with tdTomato (RFP). One week after the final tamoxifen dose, we started the mice on a five-week 0.2% cuprizone diet to induce demyelination. Control mice were fed regular chow for the same time period. After five weeks, the cuprizone-fed mice were returned to their regular chow for a two-week recovery period to allow for spontaneous remyelination, while the control mice remained on regular diet (Figure 3a).

As expected, we found very few, if any, RFP+ fate-mapped cells in corpus callosum of the regular diet fed mice of either genotype (Figure 3e, 3f). However, there was a significant ~53-fold increase in the RFP+ cells in the corpus callosum of $Gli1^{HET}$;$Gpr62^{KO}$ mice upon demyelination (38.76 +/-6.48) compared to the regular diet-fed mice (0.73 +/-0.46), and a 2.5-fold significant increase over the cuprizone-fed $Gli1^{HET}$;$Gpr62^{WT}$ mice (14.48 +/- 5.43) (Figure 3f). Since genetic loss of Gli1 enhances remyelination, we examined the effect of loss of Gpr62 in Gli1-knockout mice upon demyelination. To obtain Gli1-knockout mice, we bred the knock-in $Gli1^{CreERT}$ mice to homozygosity and generated $Gli1^{NULL}$;$Gpr62^{WT}$ mice ($Gli1^{CreERT/CreERT}$;Ai9) and $Gli1^{NULL}$;$Gpr62^{KO}$ mice ($Gli1^{CreERT/CreERT}$;$Gpr62^{-/-}$;Ai9) mice. Interestingly, the number of RFP+ cells in the corpus callosum of cuprizone-fed $Gli1^{HET}$;$Gpr62^{KO}$ mice (38.76 +/-6.48) was similar to that in the cuprizone-fed $Gli1^{NULL}$;$Gpr62^{WT}$ mice (63.08 +/-16.62), suggesting that loss of Gpr62 phenocopies the effect of loss of Gli1 in enhancing the recruitment of NSC derived cells to the corpus callosum upon demyelination (Figure 3f). As expected, there were a higher number of RFP+ cells in the corpus callosum of cuprizone-fed $Gli1^{NULL}$;$Gpr62^{WT}$ mice (63.08 +/-16.62) compared to $Gli1^{HET}$;$Gpr62^{WT}$ mice (14.48 +/-5.43) fed with cuprizone diet, consistent with our prior results (24). However there was no significant difference between the number of RFP+ cells in the corpus callosum of cuprizone-fed $Gli1^{NULL}$;$Gpr62^{KO}$ mice (57.93 +/-17.39) compared to $Gli1^{NULL}$;$Gpr62^{WT}$ mice (63.08 +/-16.62) fed with cuprizone diet, suggesting that combined loss of Gli1 and Gpr62 does not have a synergistic effect on recruitment of NSC derived cells to the lesion.

(Figure 3f).

To examine the fate of the recruited RFP+ cells in the corpus callosum, we used immunofluorescent staining to identify CC1+ mature OLs and NG2+ oligodendrocyte progenitor cells co-expressing RFP. We found no significant difference between the percentage of RFP+CC1+ oligodendrocytes in the $Gli1^{HET}$;$Gpr62^{WT}$ mice (27.37% +/- 0.433%) and the $Gli1^{HET}$;$Gpr62^{KO}$ mice (24.80% +/-6.66%) upon demyelination (Fig. 3g). However, we did find a significant decrease in the percentage of RFP+NG2+ OPCs in the $Gli1^{NULL}$;$Gpr62^{WT}$ mice (5.22% +/-2.62%) compared to $Gli1^{HET}$;$Gpr62^{WT}$ mice (22.82% +/- 3.76) suggesting that either delayed maturation of Gli1 NSC derived OPCs or increase in their survival and/or proliferation in the $Gli1^{HET}$;$Gpr62^{WT}$ mice (Fig 3h). However, there was no change in the percentage of RFP+NG2+ OPCs between $Gli1^{HET}$;$Gpr62^{KO}$ and $Gli1^{NULL}$;$Gpr62^{KO}$ mice. Together these results suggest that loss of Gpr62 changes the recruitment of Gli1 NSC-derived progeny from the SVZ to the demyelination site and that it appears to function independently of Gli1 loss. While the percentage of fate-mapped OLs in the CC did not change in the $Gli1^{HET}$;$Gpr62^{KO}$ mice, the overall increase in fate-mapped cells resulted in an overall increase in OLs in the cuprizone-damaged CCs.

After observing the increased recruitment and differentiation of Gli1+ NSCs upon global loss of Gpr62, we wanted to examine the cell-autonomous effects of Gpr62 in NSCs. For this, we conditionally knocked out Gpr62 specifically in Gli1+ NSCs in adult mice by crossing our $Gli1^{CreER/+}$; $Ai9^{Fx}$ mice with the $Gpr62^{Fx/Fx}$ mice developed by the Emery Lab at Oregon Health and Science University and described in Hay, et. al., 2021 (103). We injected four $Gli1^{CreER/+}$;$Gpr62^{Fx/Fx}$;$Ai9^{Fx}$ mice ($Gli1^{HET}$;$Gpr62^{FX}$) and four $Gli1^{CreER/+}$;$Ai9^{Fx}$ mice ($Gli1^{HET}$;$Gpr62^{WT}$) mice with tamoxifen at 8-12 weeks of age to

knock out Gpr62 in Gli1+ NSCs and permanently label them with tdTomato (RFP). A week after the final tamoxifen dose, we fed them a diet of 0.2% cuprizone for five weeks to induce demyelination while the healthy control mice were fed regular chow. This was followed by a period of two weeks on regular diet for remyelination recovery (Figure 5a). Our results showed a striking increase in the number of RFP+ cells in the $Gli1^{HET}$; $Gpr62^{FX}$ (138.76 +/-52.4) mice compared to the $Gli1^{HET}$; $Gpr62^{WT}$ mice (14.48 +/-5.43) upon demyelination. We further bred $Gli1^{CreER/CreER}$;$Gpr62^{Fx/Fx}$;$Ai9^{Fx}$ ($Gli1^{NULL}$;$Gpr62^{FX}$) mice and these mice on the cuprizone diet did show an increase in RFP+ cells in the (156.33 +/-40.51) compared to the $Gli1^{NULL}$;$Gpr62^{WT}$ (63.08 +/-6.48) mice, however this increase was not significantly different compared to the $Gli1^{HET}$;$Gpr62^{FX}$ (138.76 +/-52.4) mice. Again, this suggests a mechanism independent from Gli1 loss.

Interestingly, most of the RFP+CC1+ mature OLs in the corpus callosum of $Gli1^{HET}$; $Gpr62^{FX}$ mice showed parallel configuration of their processes, while the $Gli1^{HET}$;$Gpr62^{WT}$ brains showed more random organization of processes, suggesting that these OLs had precociously matured into myelinating cells at two weeks after cessation of cuprizone diet (113, 114) (Figure 4f). To determine if the parallel processes in the RFP+ OLs were forming functional myelin two weeks after cessation of cuprizone, we examined the presence of Caspr+ paranodes adjacent to the RFP-labelled internodes in axons. Caspr (also known as contactin-associated protein 1, and paranodin) is a protein that is expressed by the neuronal axons at the paranodes, i.e. at the edge of the myelin wrapped internodes.

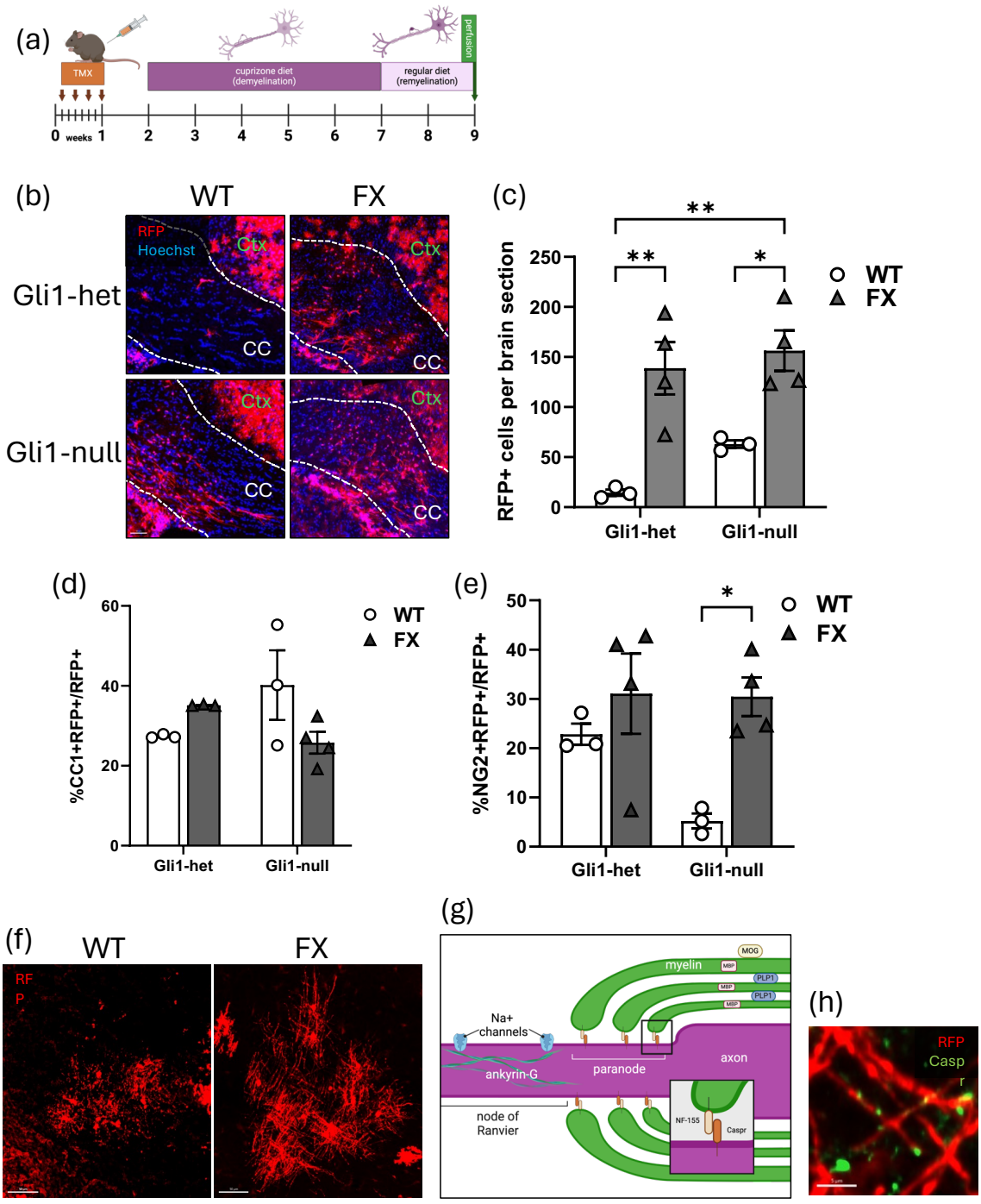

Figure 4. Conditional loss of Gpr62 in Gli1 NSCs increases oligodendrogenesis for remyelination

(a.) Timeline of remyelination experiment. (b.) Representative images of WT and FX mouse CC after 5 weeks of 0.02% cuprizone diet followed by two weeks recovery on regular diet. (Scale bar = 50 μm) (c.) Quantification of fate-mapped cells in the CC, including KO data from Fig. (Two-

way ANOVA with Tukey's post hoc test; n=3 for all except Gli1-null; FX: n=4) (d.) Representative image of CC1+RFP+ and NG2+RFP+ cells in remyelinated CC. (Scale bar = 20 μm) (e.) Percentage of remyelinating cells differentiated into mature OLs and OPCs. (Unpaired t-tests on individual cell types. (f.) Image of paired Caspr signals on RFP+ process in remyelinated CC. (Scale bar = 50 μm) (g.) Diagram of a node of Ranvier. (h.) Image of Caspr signal on RFP+ processes. (scale bar = 5 μm), WT = wildtype; FX = Gpr62 conditional knockout; CC = corpus callosum; Error bars=SEM, *$p<0.05$, **$p<0.01$, ***$p<0.001$

Caspr binds to neurofilament 155 (NF-155) expressed on the myelin edge and together they function to hold the lip of the myelin to the axon at the paranode (115, 116) (Figure 4g). As shown in Figure 4f, at two weeks of remyelination we found paired Caspr on RFP+ processes. Together these results suggest that the fate-mapped cells populating the CC two weeks following demyelination are OPCs and myelinating OLs.

CHAPTER FOUR: GPR62 KNOCKOUT RESULTS IN DIFFERENTIAL EXPRESSION OF PATHWAYS REGULATING MYELIN DEVELOPMENT

Gpr62 knockout alters myelin signaling pathways

Gpr62 has been shown in previous studies to constitutively activate cAMP (42, 62, 117). cAMP is well-known to be integral to OL differentiation and maturation, and cAMP analogs are commonly used to induce OL differentiation in vitro (68, 71, 74). To determine if cAMP is responsible for the increased maturation of oligodendrocytes seen in NSC differentiation, we induced cAMP activity by forskolin treatment in NSCs in vitro. In cells, cAMP is produced by adenylate cyclase (AC) which is activated by $G_{\alpha s}$ protein action downstream of GPCRs. The diterpene forskolin is used to stimulate AC in cultured cells (118, 119). Forskolin directly activates AC which leads to an increase in intracellular cAMP. We harvested NSCs from the SVZ of adult Gpr62-WT (WT) and Gpr62-KO (KO) mice and differentiated them in the presence of 10μM forskolin or vehicle for 14 days. Subsequently, the cells were fixed and immunofluorescent stained with antibodies against the myelin proteins PLP1 and MBP (Figure 5a). Although we found no significant change in the percentage of WT cells generating PLP1+ OLs in the vehicle-treated cells (2.04% +/-0.778%) compared to the forskolin-treated (1.98% +/-0.784%) (Figure 5b), nor in the KO cells between vehicle-treated (3.25% +/-0.981%) and forskolin treated (3.85% +/-0.258%); there was a significantly higher proportion of PLP1+ OLs that co-expressed MBP in the vehicle-treated KO cells (25.5% +/-7.78%) compared to the vehicle-treated WT cells (8.62% +/-3.62%) (Figure 6c). This suggests that Gpr62-KO OLs are more mature than

WT OLs. However, when the NSCs were differentiated with 10μM forskolin, the proportion of MBP+PLP+ KO cells (7.92% +/-5.17%) remained similar to the WT cells (12.7% +/-8.14%). This suggests that the constitutive activation of cAMP by Gpr62 inhibits the precocious maturation of OLs.

To assess the effect of global loss of Gpr62 on gene expression in the mouse brain, we performed a bulk RNA-seq transcriptomic analysis of WT vs Gpr62-KO forebrains. Of the more than 12,000 genes expressed in the forebrains of mice, 276 were unique to the WT brain and 312 were uniquely expressed in the Gpr62-KO brain (Figure 5d). The RNA-seq analysis revealed 39 differentially expressed genes between WT and KO mice at a false discovery rate (FDR) of 0.01 (Table 2). Of these, 32 were upregulated and seven genes were downregulated in the Gpr62-KO brain (Figure 5e). Among the top five differentially expressed genes was Fatty Acid Binding Protein 7 (Fabp7) which was upregulated in the Gpr62-KO brains (Figure 5f, Table 2). Fabp7 has previously been shown to be necessary for developmental oligodendrocyte differentiation (7, 120). A previous study found Fabp7 to be dispensable in remyelination (7), however, this study focused on remyelination by OPCs in the spinal cord and did not examine remyelination by NSCs in the brain.

To confirm the RNA-seq finding, we performed qPCR with mRNA extracted from the WT and Gpr62-KO forebrain and found a two-fold increase in Fabp7 expression in the Gpr62-KO mice (+1.9 +/-0.18 fold change) (Figure 5g.). Further work will need to be done to determine the exact role Fabp7 plays in regulating the path from NSC to OL in remyelination.

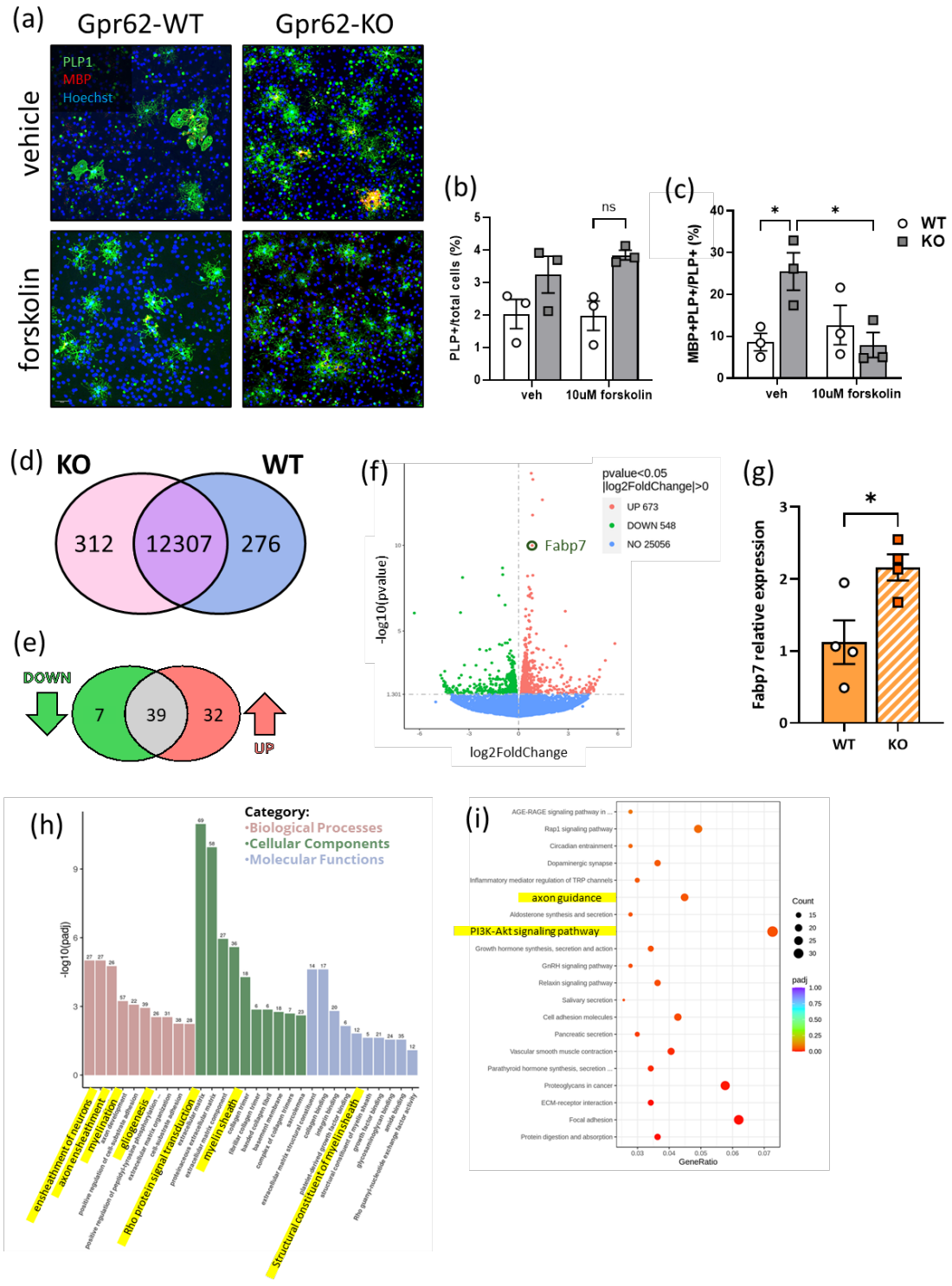

Figure 5. Loss of Gpr62 alters signaling pathways regulating myelination.

(a.) Representative images of MBP+PLP+ cells in forskolin-treated, 14-day differentiated WT and KO NSCs (Scale bar = 50 μm) (b.) Percentage of PLP+/total cells in forskolin-treated differentiated WT and KO NSCs. (Two-way ANOVA with Tukey's post hoc test; n=3) (c.) Percentage of MBP+PLP+/PLP+ cells cells in forskolin-treated differentiated WT and KO NSCs. (Two-way ANOVA with Tukey's post hoc test; n=3) (d.) Venn diagram comparing mRNA expression in KO and WT mouse forebrains analyzed by RNA-seq. (e.) Venn diagram of differentially expressed genes from RNA-seq of KO vs. WT mouse forebrains. (f.) Volcano plot of differentially expressed genes from RNA-seq of KO vs. WT mouse forebrains, highlighting Fabp7. (g.) RT-qPCR of Fabp7 in mouse forebrains (n=4). (h.) GO analysis for KO vs. WT mouse forebrain. Myelin-related pathways highlighted in yellow. (i.) KEGG pathway enrichment analysis of KO vs. WT mouse forebrain. Myelin-related pathways highlighted in yellow. WT = wildtype; KO = Gpr62-knockout; NSCs = neural stem cells; GO = Gene Ontology; Error bars=SEM, *$p<0.05$, **$p<0.01$, ***$p<0.001$, n/s = not significant

As part of the RNA-seq analysis on Gpr62-KO forebrains, we performed a gene ontology (GO) pathway analysis and Kyoto Encyclopedia of Genes and Genomes (KEGG) pathway analysis. Strikingly, the GO analysis with differentially expressed genes identified several pathways relating to myelin development, including myelination, neuron/axon ensheathment, gliogenesis, myelin sheath, and myelin sheath structure (Fig. 5h.). Similarly, the KEGG analysis identified the axon guidance pathway, as well as PI3K-Akt signaling pathway (Fig. 5i), which has been shown to regulate myelin sheath growth (121). Unexpectedly for a Class-A Rhodopsin GPCR (as opposed to Adhesion GPCRs), we found many pathways related to extracellular matrix (ECM) components and binding represented in the GO and Kegg analysis. This presents an intriguing avenue for future research, as ECM proteins are involved in regulating OL development and myelination. A summary of the pathways related to ECM is shown in Figures 5h and 5i.

Table 2. Differentially expressed genes in Gpr62-KO forebrain.

log2 fold change	padj	gene name
2.827378921	0.000476	Gm26747
1.440265538	1.13E-09	Eln
1.076493953	0.00708	Hpgd
0.863664039	1.10E-10	Tspan2
0.861871292	1.07E-05	Fabp7
0.84681677	6.63E-09	Cldn11
0.825600184	9.87E-05	Smim3
0.822172527	3.15E-07	Gpr17
0.807787049	0.000466	Mcam
0.772176725	7.49E-05	Ugt8a
0.767379538	9.63E-11	Mal
0.732011798	0.003384	Mfsd2a
0.698796679	0.003938	Igsf1
0.692289581	4.75E-05	Elovl1
0.687360167	8.03E-05	Gsn
0.680638557	8.03E-05	Col6a1
0.673018407	8.56E-05	Mog
0.656771833	0.001534	Col6a2
0.654525135	0.010497	Srd5a1
0.641807731	0.007713	Adamts4
0.634696322	0.000729	Mag
0.623085649	3.90E-05	Plp1
0.613362652	0.001393	Lpar1
0.576223701	8.03E-05	Mobp
0.543579514	1.07E-05	Cnp
0.524657517	0.003871	Fa2h
0.436151431	0.012602	Sema4d
0.434962824	0.00039	Dusp26
0.425246347	0.000834	Marcksl1
0.414690118	0.011562	Sh3gl3
0.400438543	0.013778	Sirt2
0.353651713	0.013778	Adgrg1
-0.530054542	0.013566	Plk5
-0.816685807	0.000237	Il33
-0.960990534	1.07E-05	Gm29216
-0.973503082	5.40E-06	Gpr62
-1.196549954	8.03E-05	Ahcyl
-3.394780899	1.17E-05	Gm35021
-3.516931765	0.000545	Gm7292

CHAPTER FIVE: DISCUSSION AND FUTURE DIRECTIONS

Discussion

Given the high expression of Gpr62 in myelinating oligodendrocytes and its localization in the brain and testes, it would be natural to expect that it would have some role in regulating myelination and/or spermatogenesis. However, previous work has determined that Gpr62 is not needed for developmental central nervous system (CNS) myelination (103), nor does its loss affect spermatogenesis (62). Taking these findings into consideration, a logical step is to next look at its role in remyelination. Remyelination in the CNS can occur from a few different cell populations: the surviving oligodendrocytes in the area of the demyelinated lesion (19), the resident oligodendrocyte progenitor cells (OPCs) (17, 23, 43), or the neural stem cells (NSCs) of the subventricular zone (SVZ) (24, 122, 123). Having previously established that the Gli1+ NSCs of the SVZ are particularly responsive to demyelination (24), we endeavored to examine the role of Gpr62 in remyelination. First, we confirmed the expression of Gpr62 in myelinating oligodendrocytes and found significant increases in areas of the brain enriched with myelinating oligodendrocytes, as well as in normal brain tissue compared to cuprizone-demyelinated tissue which coincides with studies showing Gpr62 expression increasing as oligodendrocytes mature (34, 35, 103).

Using a cell culture model of neural stem cell differentiation, we found significant morphological changes in oligodendrocytes after 14 days of differentiation when Gpr62 is

lost. Additionally, we found an increase in OPCs in cells where Gpr62 is knocked out. This correlated with a two-fold increase in NG2 expression in the knockout cells. We did not see a significant change in the percentage of NSCs differentiating into PLP+ OLs in the KO compared to WT, however we did find an increase in the PLP+ OLs that were also expressing MBP, as well as an almost three-fold increase in MBP expression in KO over WT cultured cells. This would again suggest a more rapidly maturing OL population with the loss of Gpr62, as the onset of MBP expression is a commonly used marker for mature OLs (68, 69, 124).

Using Scholl analysis, we determined that the differentiated PLP+ OLs demonstrated higher order process branching, which is indicative of higher OL maturity (109). Conversely, when we virally overexpressed Gpr62 in differentiating neural stem cells, we found very few OLs generated from the Gpr62 overexpressing cells. Those few that we did find appeared to have lower expression of the viral Gpr62, and their morphology showed stunted process growth. Cells of any type that were highly expressing viral Gpr62 had no discernable process branching. This suggests a role for Gpr62 in controlling precocious maturation or process branching. Other GPCRs are critical in controlling the rate of maturation and regulating the commitment of stem cells to the OL lineage. A role for Gpr62 in maturation regulation is in line with other GPCR activity in myelination (39, 47, 48, 52).

The early maturation of Gpr62 knockout NSCs in culture appears to extend into *in vivo* NSCs responding to demyelination, particularly in the CC. Our findings that loss of Gpr62 leads to a significant increase in cells migrating to the corpus callosum from the

SVZ, appear to mirror those previously reported by our lab on the effect of loss of Gli1. Loss of Gpr62 appears to have a comparable effect on remyelinating cells to that observed upon pharmacological and genetic ablation of Gli1 (24). We did not find a combinatorial effect of Gli1 and Gpr62 global knockout. However, when we conditionally knocked out Gpr62 in Gli1+ NSCs, we did see an additive effect of combined loss of Gli1 and Gpr62. This resulted in a significant increase in the number of NSCs responding to, and migrating to the site of demyelination in the CC.

Future Directions

Gpr62 offers several directions for future research. A key direction is to find the endogenous ligand for Gpr62. While C1q has been reported as binding to Gpr62, thus far this pairing has not been shown to have biological relevance. Examining the effects of C1q on Gpr62 signaling could open up further avenues for drug discovery. Along with the endogenous ligand, another important avenue is to elucidate the particular mechanism of Gpr62's constitutive activity in mature oligodendrocytes.

Of particular interest stemming from the findings in this work is the specific means by which Gpr62 regulates process branching.

In light of the pathway analyses that indicate Gpr62's affiliation with ECM signaling, it appears to be crucial to understand what role Gpr62 might play in interacting with the ECM. The stiffness of the ECM affects many pathways, including OL

differentiation. A number of proteins involved in sensing the ECM are also key players in process extension; among them are Rho/ROCK and filamental actin. (109, 125)

We have recently begun a collaboration investigating the effect of Gpr62 loss on extracellular vesicles secreted by differentiating NSCs. Our preliminary results indicate differences in both size and number of EVs secreted by Gpr62-KO cells compared to WT. Quantifying and characterizing these EVs and their cargoes could lead to further understanding of Gpr62's role in regulating OL differentiation and maturation. As previous work has suggested Gpr62's localization as being either on the adaxonal surface of the myelin sheath or in the proximal ends of the processes, a key avenue for future research would be to find the precise locale of Gpr62 (55, 103). Our viral overexpression experiments suggest an endosomal membrane concentration, as well as a lesser plasma membrane expression. Developing an antibody that works in mouse tissue would be a large leap forward in Gpr62 research.

CHAPTER SIX: METHODS & MATERIALS

Animals

The Cre-knockin line *Gli1*^{CreERT}; *Ai9*^{FX} was generated by crossing *Gli1*^{CreERT} line (Jackson Labs #007913) with the *Ai9*^{FX} reporter line (Jackson Labs #007909). *Gpr62*$^{-/-}$ mice were bred by inseminating C57Bl/6 WT female mice with *Gpr62*$^{-/-}$ sperm gifted by the Keiichiro Yogo lab at Shizuoka University, Shizuoka, Japan. The Yogo lab's generation of the *Gpr62*$^{-/-}$ line is described in Muroi, 2017 (62). *Gli1*$^{CreER/WT}$; *Gpr62*$^{-/-}$; *Ai9*$^{FX/WT}$ were generated by crossbreeding *Gpr62*$^{-/-}$ mice with *Gli1*^{CreERT}; *Ai9*^{FX} mice.

Mice for early experiments were housed at the UW-Madison School of Veterinary Medicine vivarium and cared for according to the IACUC protocol. Due to a lab move, later experimental mice were housed at the UGA College of Veterinary Medicine animal facility and cared for according to IACUC protocol. A mix of male and female animals were used in all experiments.

Cre-mediated fate-mapping

Mice with the Cre-knockin *Gli1*^{CreERT}; *Ai9*^{FX} were given four 250 µl doses of 20 mg/ml Tamoxifen dissolved in corn oil delivered via i.p. injection every other day for a total of 1 ml tamoxifen per mouse. All subsequent experiments with tamoxifen-dosed mice were started one week following the last dose of tamoxifen.

Cuprizone-mediated demyelination

Mice were fed 0.2% Cuprizone chow diet (Inovtiv custom diet) ad libitum for 5 weeks to induce acute demyelination. The mice were perfused as described below, and brains were collected at this point to assess the extent of demyelination. For remyelination analysis, mice were fed a 0.2% cuprizone diet for five weeks followed by two weeks of their regular diet. Control mice were fed their regular diet for the duration.

NSC harvest and differentiation

Neural stem cell harvest and culture were performed as previously described in Radecki, et. al., 2022 (108). In brief, mice were anesthetized, and brains were collected and sliced into 1mm slices in a brain mold. Under a dissecting microscope, the SVZs of the slices were cut out, diced, and digested in 0.25% trypsin for 5 min. @ 37 °C and the trypsin deactivated with trypsin inhibitor. The tissue was then triturated with a 25Ga needle and 3ml syringe. This was followed by centrifugation @500xg for 5 min. and resuspension of the pellet in proliferation media (Stem Cell Technologies #05702) supplemented with heparin, FGF, and EGF for growth into neurospheres. Neurospheres were passaged two times before plating the tertiary neurospheres. For plating, tertiary neurospheres were disassociated in 0.25% trypsin for 5 min @37 °C and counted using a BioRad TC20 Automated Cell Counter. Cells were plated on either matrigel-coated cell culture plates or matrigel-coated 12 mm coverslips in 24-well plates at $1.2x10^6$ cells per plate. Cells were cultured in differentiation media (Stem Cell Technologies #05704) supplemented with antibiotic-antimycotic (Thermo Fisher #15240062), heparin, FGF, and EGF. Media was

changed every other day for fourteen days. Cells for immunofluorescent staining were then fixed with ice-cold methanol for 15 min, followed by 3x washes with RT PBS. Cells for qPCR were lifted with 0.25% trypsin for 5 min @37 °C, followed by deactivation with trypsin inhibitor, then centrifuged @500xg for 5 min and resuspended in RNA later (Thermo Fisher #AM7020).

Mouse Brain Harvest

Mouse brains were harvested, sectioned, and stained as previously described in Clawson, et. al., 2023 (126). In brief, mice were perfused via cardiac puncture with 4% PFA in PBS. Brains were harvested and post-fixed for four hours @4 °C, followed by overnight incubation in 30% sucrose-PBS solution. Brains were embedded in OCT media in a tissue mold and frozen at -80 °C.

Immunofluorescent tissue staining (refer to paper)

20um thick cryosectioned brain slices on microscope slides or cultured cells on coverslips were incubated in ice-cold methanol for 15 minutes @RT for myelin protein staining. Slides were blocked with 1:10 dilution of normal goat serum for 1 hour @RT. Primary antibodies were incubated overnight @4 °C, in 0.1%BSA-PBS-TritonX solution. Primary antibodies used: rat anti-PLP 1:50 (Macklin Lab OHSU), CC1 1:100 (Calbiochem #OP80), NG2 Millipore #AB5320), β-III tubulin (Tuj1) 1:200 (R&D Systems #MAB1195), MBP 1:100 (Biolegend #808402), GFAP 1:500 (NovusBio #NBP2-29415), RFP 1:1000 (Chromotek #5F8-100), GFP 1:1000 (Invitrogen #A10262). Fluorescent goat

secondary antibodies in 0.1%BSA-PBS-TritonX were incubated for 1 hr. @RT. Secondary Antibodies: all at 1:1000 dilution. After 3x washing in PBS, coverslips were mounted with FluoromountG (Thermo Fisher #00-4958-02). Slides were imaged with a Keyence X-700 epifluorescent microscope or Oxford Instruments BC43 Benchtop Confocal and analyzed using Fiji or Imaris software.

Scholl analysis

Using Fiji, images of oligodendrocytes were cropped to isolate the cell from surrounding cells, threshold set by hand to remove background noise and any processes from surrounding cells, then skeletonized using the Skeletonize function of the Neuroanatomy Shortcuts Tool for Fiji. The distance from the center of the nucleus to the end of the longest process was measured in Fiji to use as the Scholl diameter. Then using the Scholl analysis function of the Neuroanatomy Shortcuts Tool, the OLs were analyzed using the previously calculated diameter at 1 μm intervals starting at 5 μm from center. A minimum of 25 cells from each replicate were analyzed, for a total per genotype of 100 cells.

RT-qPCR

RNA was purified using the Monarch Total RNA Miniprep kit (NEB #T2010S) and quantified using a Qubit 4 Fluorometer. cDNA was synthesized using iScript cDNA Synthesis kit (BioRad # 1708890), and qPCR was performed using SsoAdvanced

Universal SYBR Green Supermix (BioRad # 1725271) in a BioRad Optum96 with the following primers listed in Table 3.

Table 3. qPCR primer sequences

Cspg4/NG2	F: CTTCACGATCACCATCCTTCC R: CCCGAATCATTGTCTGTTCCC
EGFR	F: CCCGAATCATTGTCTGTTCCC R: TGTCTTCACCAGTACATTCCTG
Fabp7	F: GAAGTGGGATGGCAAAGAAAC R: CATAACAGCGAACAGCAACG
Gapdh	F: AATGGTGAAGGTCGGTGTG R: GTGGAGTCATACTGGAACATGTAG
Gpr62	F: CCTGCTGGCTGCCTTAT R: GCAGCAGGCCATAGAGAAA
MBP	F: GCCTTGCCAGTTATTCTTTGG R: CTCAGAGGACAGTGATGTGTT
Plk5	F: GCAACCAGAAAACTGTTCCT R: GTAGCCGAAGCCATACTTGAG
Tspan2	F: AGAGGTGATGAGAAGAGGAGA R: CAAATGCAATAACGGCTGATCC

RNA-seq

Brains were harvested from two male and two female each of WT and Gpr62-KO mice at 8-10 weeks of age after euthanizing with pentobarbital. The forebrains were minced and stored at -20°C in RNA Later. The tissue was shipped to Novogene on dry ice where the bulk RNAseq and analysis was performed.

In brief, Novogene purified the mRNA using magnetic beads with attached poly-T oligos, followed by reverse transcription and second strand cDNA synthesis. After library prep and quantification, the cDNA was PCR amplified. Novogene then performed quality control using their in-house perl scripts. They used Hisat2 (v2.0.5) to build the reference

genome index, and novel transcripts were predicted using StringTie (v1.3.3b). Gene expression levels were quantified using FeatureCounts v1.5.0-p3. Differential expression analysis comparing WT vs. Gpr62-KO was done with the DESeq2R (v1.20.0) package. GO and KEGG analysis were performed using clusterProfiler R package.

Statistical Analysis

Statistical Analysis was performed using Prism software. Specific tests performed are listed in the corresponding figure legends.

REFERENCES

1. Zalc B. The acquisition of myelin: An evolutionary perspective. Brain Res. 2016;1641(Pt A):4-10. Epub 20150911. doi: 10.1016/j.brainres.2015.09.005. PubMed PMID: 26367449.

2. Chong SY, Rosenberg SS, Fancy SP, Zhao C, Shen YA, Hahn AT, et al. Neurite outgrowth inhibitor Nogo-A establishes spatial segregation and extent of oligodendrocyte myelination. Proc Natl Acad Sci U S A. 2012;109(4):1299-304. Epub 20111212. doi: 10.1073/pnas.1113540109. PubMed PMID: 22160722; PubMed Central PMCID: PMC3268264.

3. Hartline DK, Colman DR. Rapid Conduction and the Evolution of Giant Axons and Myelinated Fibers. Current Biology. 2007;17(1):R29-R35. doi: https://doi.org/10.1016/j.cub.2006.11.042.

4. Woelk H, Borri P. Lipid and fatty acid composition of myelin purified from normal and MS brains. Eur Neurol. 1973;10(4):250-60. doi: 10.1159/000114281. PubMed PMID: 4778382.

5. Norton WT, Poduslo SE. Myelination in rat brain: changes in myelin composition during brain maturation. J Neurochem. 1973;21(4):759-73. doi: 10.1111/j.1471-4159.1973.tb07520.x. PubMed PMID: 4754856.

6. Owada Y, Yoshimoto T, Kondo H. Spatio-temporally differential expression of genes for three members of fatty acid binding proteins in developing and mature rat brains. J Chem Neuroanat. 1996;12(2):113-22. doi: 10.1016/s0891-0618(96)00192-5. PubMed PMID: 9115666.

7. Foerster S, Guzman de la Fuente A, Kagawa Y, Bartels T, Owada Y, Franklin RJM. The fatty acid binding protein FABP7 is required for optimal oligodendrocyte differentiation during myelination but not during remyelination. Glia. 2020;68(7):1410-20. Epub 20200204. doi: 10.1002/glia.23789. PubMed PMID: 32017258; PubMed Central PMCID: PMC7317849.

8. Fünfschilling U, Supplie LM, Mahad D, Boretius S, Saab AS, Edgar J, et al. Glycolytic oligodendrocytes maintain myelin and long-term axonal integrity. Nature. 2012;485(7399):517-21. Epub 20120429. doi: 10.1038/nature11007. PubMed PMID: 22622581; PubMed Central PMCID: PMC3613737.

9. Lee Y, Morrison BM, Li Y, Lengacher S, Farah MH, Hoffman PN, et al. Oligodendroglia metabolically support axons and contribute to neurodegeneration. Nature. 2012;487(7408):443-8. doi: 10.1038/nature11314. PubMed PMID: 22801498; PubMed Central PMCID: PMC3408792.

10. Ye J, Wan H, Chen S, Liu GP. Targeting tau in Alzheimer's disease: from mechanisms to clinical therapy. Neural Regen Res. 2024;19(7):1489-98. Epub 20230922.

doi: 10.4103/1673-5374.385847. PubMed PMID: 38051891; PubMed Central PMCID: PMC10883484.

11. Yang Y, Zhang Z. α-Synuclein pathology from the body to the brain: so many seeds so close to the central soil. Neural Regen Res. 2024;19(7):1463-72. Epub 20231108. doi: 10.4103/1673-5374.387967. PubMed PMID: 38051888; PubMed Central PMCID: PMC10883481.

12. Kuhlmann T, Moccia M, Coetzee T, Cohen JA, Correale J, Graves J, et al. Multiple sclerosis progression: time for a new mechanism-driven framework. Lancet Neurol. 2023;22(1):78-88. Epub 20221118. doi: 10.1016/s1474-4422(22)00289-7. PubMed PMID: 36410373; PubMed Central PMCID: PMC10463558.

13. Kular L, Jagodic M. Epigenetic insights into multiple sclerosis disease progression. J Intern Med. 2020;288(1):82-102. Epub 2020/07/03. doi: 10.1111/joim.13045. PubMed PMID: 32614160.

14. Duncan ID, Brower A, Kondo Y, Curlee JF, Jr., Schultz RD. Extensive remyelination of the CNS leads to functional recovery. Proc Natl Acad Sci U S A. 2009;106(16):6832-6. Epub 20090402. doi: 10.1073/pnas.0812500106. PubMed PMID: 19342494; PubMed Central PMCID: PMC2672502.

15. El Waly B, Macchi M, Cayre M, Durbec P. Oligodendrogenesis in the normal and pathological central nervous system. Frontiers in Neuroscience. 2014;8(145). doi: 10.3389/fnins.2014.00145.

16. Elbaz B, Popko B. Molecular Control of Oligodendrocyte Development. Trends in Neurosciences. 2019;42(4):263-77. doi: 10.1016/j.tins.2019.01.002.

17. Menn B, Garcia-Verdugo JM, Yaschine C, Gonzalez-Perez O, Rowitch D, Alvarez-Buylla A. Origin of Oligodendrocytes in the Subventricular Zone of the Adult Brain. The Journal of Neuroscience. 2006;26(30):7907-18. doi: 10.1523/jneurosci.1299-06.2006.

18. Doetsch F, Caillé I, Lim DA, García-Verdugo JM, Alvarez-Buylla A. Subventricular Zone Astrocytes Are Neural Stem Cells in the Adult Mammalian Brain. Cell. 1999;97(6):703-16. doi: 10.1016/S0092-8674(00)80783-7.

19. Duncan ID, Radcliff AB, Heidari M, Kidd G, August BK, Wierenga LA. The adult oligodendrocyte can participate in remyelination. Proceedings of the National Academy of Sciences. 2018;115(50):E11807-E16. doi: 10.1073/pnas.1808064115.

20. Yeung MSY, Djelloul M, Steiner E, Bernard S, Salehpour M, Possnert G, et al. Dynamics of oligodendrocyte generation in multiple sclerosis. Nature. 2019;566(7745):538-42. doi: 10.1038/s41586-018-0842-3.

21. Neely SA, Williamson JM, Klingseisen A, Zoupi L, Early JJ, Williams A, et al. New oligodendrocytes exhibit more abundant and accurate myelin regeneration than those that survive demyelination. Nat Neurosci. 2022;25(4):415-20. Epub 20220214. doi: 10.1038/s41593-021-01009-x. PubMed PMID: 35165460; PubMed Central PMCID: PMC7612594.

22. Mezydlo A, Treiber N, Ullrich Gavilanes EM, Eichenseer K, Ancău M, Wens A, et al. Remyelination by surviving oligodendrocytes is inefficient in the inflamed mammalian cortex. Neuron. 2023;111(11):1748-59.e8. doi: https://doi.org/10.1016/j.neuron.2023.03.031.

23. Serwanski DR, Rasmussen AL, Brunquell CB, Perkins SS, Nishiyama A. Sequential Contribution of Parenchymal and Neural Stem Cell-Derived Oligodendrocyte Precursor Cells toward Remyelination. Neuroglia. 2018;1(1):91-105. Epub 2019/01/22. doi: 10.3390/neuroglia1010008. PubMed PMID: 30662979; PubMed Central PMCID: PMC6335037.

24. Samanta J, Grund EM, Silva HM, Lafaille JJ, Fishell G, Salzer JL. Inhibition of Gli1 mobilizes endogenous neural stem cells for remyelination. Nature. 2015;526(7573):448-52. Epub 2015/09/30. doi: 10.1038/nature14957. PubMed PMID: 26416758.

25. Windrem MS, Schanz SJ, Zou L, Chandler-Militello D, Kuypers NJ, Nedergaard M, et al. Human Glial Progenitor Cells Effectively Remyelinate the Demyelinated Adult Brain. Cell Reports. 2020;31(7):107658. doi: https://doi.org/10.1016/j.celrep.2020.107658.

26. Crawford AH, Tripathi RB, Foerster S, McKenzie I, Kougioumtzidou E, Grist M, et al. Pre-Existing Mature Oligodendrocytes Do Not Contribute to Remyelination

following Toxin-Induced Spinal Cord Demyelination. The American Journal of Pathology. 2016;186(3):511-6. doi: 10.1016/j.ajpath.2015.11.005.

27. Blakemore WF, Keirstead HS. The origin of remyelinating cells in the central nervous system. Journal of Neuroimmunology. 1999;98(1):69-76. doi: https://doi.org/10.1016/S0165-5728(99)00083-1.

28. Bacmeister CM, Barr HJ, McClain CR, Thornton MA, Nettles D, Welle CG, et al. Motor learning promotes remyelination via new and surviving oligodendrocytes. Nat Neurosci. 2020;23(7):819-31. Epub 20200518. doi: 10.1038/s41593-020-0637-3. PubMed PMID: 32424285; PubMed Central PMCID: PMC7329620.

29. Zawadzka M, Rivers LE, Fancy SP, Zhao C, Tripathi R, Jamen F, et al. CNS-resident glial progenitor/stem cells produce Schwann cells as well as oligodendrocytes during repair of CNS demyelination. Cell Stem Cell. 2010;6(6):578-90. doi: 10.1016/j.stem.2010.04.002. PubMed PMID: 20569695; PubMed Central PMCID: PMC3856868.

30. Duncan ID, Marik RL, Broman AT, Heidari M. Thin myelin sheaths as the hallmark of remyelination persist over time and preserve axon function. Proc Natl Acad Sci U S A. 2017;114(45):E9685-e91. Epub 20171024. doi: 10.1073/pnas.1714183114. PubMed PMID: 29078396; PubMed Central PMCID: PMC5692595.

31. Samanta J, Salzer JL. Transcriptomic analysis of loss of Gli1 in neural stem cells responding to demyelination in the mouse brain. bioRxiv. 2021:2021.02.28.433246. doi: 10.1101/2021.02.28.433246.

32. Ayoglu B, Mitsios N, Kockum I, Khademi M, Zandian A, Sjöberg R, et al. Anoctamin 2 identified as an autoimmune target in multiple sclerosis. Proceedings of the National Academy of Sciences. 2016;113(8):2188-93. doi: 10.1073/pnas.1518553113.

33. Ayoglu B, Häggmark A, Khademi M, Olsson T, Uhlén M, Schwenk JM, et al. Autoantibody profiling in multiple sclerosis using arrays of human protein fragments. Mol Cell Proteomics. 2013;12(9):2657-72. Epub 2013/06/05. doi: 10.1074/mcp.M112.026757. PubMed PMID: 23732997; PubMed Central PMCID: PMC3769337.

34. Zhang Y, Chen K, Sloan SA, Bennett ML, Scholze AR, O'Keeffe S, et al. An RNA-Sequencing Transcriptome and Splicing Database of Glia, Neurons, and Vascular Cells of the Cerebral Cortex. The Journal of Neuroscience. 2014;34(36):11929-47. doi: 10.1523/jneurosci.1860-14.2014.

35. Cahoy JD, Emery B, Kaushal A, Foo LC, Zamanian JL, Christopherson KS, et al. A Transcriptome Database for Astrocytes, Neurons, and Oligodendrocytes: A New Resource for Understanding Brain Development and Function. The Journal of Neuroscience. 2008;28(1):264-78. doi: 10.1523/jneurosci.4178-07.2008.

36. Hawrylycz MJ, Lein ES, Guillozet-Bongaarts AL, Shen EH, Ng L, Miller JA, et al. An anatomically comprehensive atlas of the adult human brain transcriptome. Nature.

2012;489(7416):391-9. Epub 2012/09/22. doi: 10.1038/nature11405. PubMed PMID: 22996553; PubMed Central PMCID: PMC4243026.

37. Golan N, Adamsky K, Kartvelishvily E, Brockschnieder D, Möbius W, Spiegel I, et al. Identification of Tmem10/Opalin as an oligodendrocyte enriched gene using expression profiling combined with genetic cell ablation. Glia. 2008;56(11):1176-86. Epub 2008/06/24. doi: 10.1002/glia.20688. PubMed PMID: 18571792; PubMed Central PMCID: PMC2830273.

38. Bujalka H, Koenning M, Jackson S, Perreau VM, Pope B, Hay CM, et al. MYRF is a membrane-associated transcription factor that autoproteolytically cleaves to directly activate myelin genes. PLoS Biol. 2013;11(8):e1001625. Epub 2013/08/24. doi: 10.1371/journal.pbio.1001625. PubMed PMID: 23966833; PubMed Central PMCID: PMC3742440.

39. Ou Z, Sun Y, Lin L, You N, Liu X, Li H, et al. Olig2-Targeted G-Protein-Coupled Receptor Gpr17 Regulates Oligodendrocyte Survival in Response to Lysolecithin-Induced Demyelination. J Neurosci. 2016;36(41):10560-73. Epub 2016/10/14. doi: 10.1523/jneurosci.0898-16.2016. PubMed PMID: 27733608; PubMed Central PMCID: PMC6601930.

40. Khan MZ, He L. Neuro-psychopharmacological perspective of Orphan receptors of Rhodopsin (class A) family of G protein-coupled receptors. Psychopharmacology. 2017;234(8):1181-207. doi: 10.1007/s00213-017-4586-9.

41. Lagerström MC, Schiöth HB. Structural diversity of G protein-coupled receptors and significance for drug discovery. Nat Rev Drug Discov. 2008;7(4):339-57. Epub 2008/04/03. doi: 10.1038/nrd2518. PubMed PMID: 18382464.

42. Oishi A, Karamitri A, Gerbier R, Lahuna O, Ahmad R, Jockers R. Orphan GPR61, GPR62 and GPR135 receptors and the melatonin MT(2) receptor reciprocally modulate their signaling functions. Scientific reports. 2017;7(1):8990-. doi: 10.1038/s41598-017-08996-7. PubMed PMID: 28827538.

43. Carbajal KS, Miranda JL, Tsukamoto MR, Lane TE. CXCR4 signaling regulates remyelination by endogenous oligodendrocyte progenitor cells in a viral model of demyelination. Glia. 2011;59(12):1813-21. Epub 20110809. doi: 10.1002/glia.21225. PubMed PMID: 21830237; PubMed Central PMCID: PMC5025299.

44. Neves M, Perpiñá-Viciano C, Penela P, Hoffmann C, Mayor F, Jr. Modulation of CXCR4-Mediated Gi1 Activation by EGF Receptor and GRK2. ACS Pharmacology & Translational Science. 2020;3(4):627-34. doi: 10.1021/acsptsci.0c00021.

45. Yuen TJ, Johnson KR, Miron VE, Zhao C, Quandt J, Harrisingh MC, et al. Identification of endothelin 2 as an inflammatory factor that promotes central nervous system remyelination. Brain. 2013;136(4):1035-47. doi: 10.1093/brain/awt024.

46. Hammond TR, McEllin B, Morton PD, Raymond M, Dupree J, Gallo V. Endothelin-B receptor activation in astrocytes regulates the rate of oligodendrocyte regeneration during remyelination. Cell reports. 2015;13(10):2090-7.

47. Lu C, Dong L, Zhou H, Li Q, Huang G, Bai Sj, et al. G-Protein-Coupled Receptor Gpr17 Regulates Oligodendrocyte Differentiation in Response to Lysolecithin-Induced Demyelination. Scientific Reports. 2018;8(1):4502. doi: 10.1038/s41598-018-22452-0.

48. Simon K, Hennen S, Merten N, Blättermann S, Gillard M, Kostenis E, et al. The Orphan G Protein-coupled Receptor GPR17 Negatively Regulates Oligodendrocyte Differentiation via Gαi/o and Its Downstream Effector Molecules. J Biol Chem. 2016;291(2):705-18. Epub 2015/12/02. doi: 10.1074/jbc.M115.683953. PubMed PMID: 26620557; PubMed Central PMCID: PMC4705391.

49. Hirahara Y, Matsuda KI, Yamada H, Saitou A, Morisaki S, Takanami K, et al. G protein-coupled receptor 30 contributes to improved remyelination after cuprizone-induced demyelination. Glia. 2013;61(3):420-31. Epub 20121222. doi: 10.1002/glia.22445. PubMed PMID: 23281138.

50. Filardo EJ, Quinn JA, Frackelton AR, Jr., Bland KI. Estrogen action via the G protein-coupled receptor, GPR30: stimulation of adenylyl cyclase and cAMP-mediated attenuation of the epidermal growth factor receptor-to-MAPK signaling axis. Mol Endocrinol. 2002;16(1):70-84. doi: 10.1210/mend.16.1.0758. PubMed PMID: 11773440.

51. Revankar CM, Cimino DF, Sklar LA, Arterburn JB, Prossnitz ER. A transmembrane intracellular estrogen receptor mediates rapid cell signaling. Science. 2005;307(5715):1625-30. Epub 20050210. doi: 10.1126/science.1106943. PubMed PMID: 15705806.

52. Yang H-J, Vainshtein A, Maik-Rachline G, Peles E. G protein-coupled receptor 37 is a negative regulator of oligodendrocyte differentiation and myelination. Nature Communications. 2016;7(1):10884. doi: 10.1038/ncomms10884.

53. Ackerman SD, Garcia C, Piao X, Gutmann DH, Monk KR. The adhesion GPCR Gpr56 regulates oligodendrocyte development via interactions with Gα12/13 and RhoA. Nat Commun. 2015;6:6122. Epub 2015/01/22. doi: 10.1038/ncomms7122. PubMed PMID: 25607772; PubMed Central PMCID: PMC4302765.

54. Chiou B, Gao C, Giera S, Folts CJ, Kishore P, Yu D, et al. Cell type-specific evaluation of ADGRG1/GPR56 function in developmental central nervous system myelination. Glia. 2021;69(2):413-23. Epub 20200909. doi: 10.1002/glia.23906. PubMed PMID: 32902916.

55. Benavente F, Piltti K, Hooshmand MJ, Nava AA, Lakatos A, Feld BG, et al. Novel C1q receptor-mediated signaling controls neural stem cell behavior and neurorepair. eLife. 2020;9:e55732. doi: 10.7554/eLife.55732.

56. Hu QX, Dong JH, Du HB, Zhang DL, Ren HZ, Ma ML, et al. Constitutive Gαi coupling activity of very large G protein-coupled receptor 1 (VLGR1) and its regulation by PDZD7 protein. J Biol Chem. 2014;289(35):24215-25. Epub 20140624. doi: 10.1074/jbc.M114.549816. PubMed PMID: 24962568; PubMed Central PMCID: PMC4148852.

57. Stiene-Martin A, Knapp PE, Martin K, Gurwell JA, Ryan S, Thornton SR, et al. Opioid system diversity in developing neurons, astroglia, and oligodendroglia in the subventricular zone and striatum: impact on gliogenesis in vivo. Glia. 2001;36(1):78-88. PubMed PMID: 11571786; PubMed Central PMCID: PMC4303466.

58. Ebrahimi Z, Kahvandi N, Komaki A, Karimi SA, Naderishahab M, Sarihi A. The role of mGlu4 receptors within the nucleus accumbens in acquisition and expression of morphine-induced conditioned place preference in male rats. BMC Neuroscience. 2021;22(1):17. doi: 10.1186/s12868-021-00627-2.

59. Wang X, Wang M, Xu T, Feng Y, Shao Q, Han S, et al. Structural insights into dimerization and activation of the mGlu2–mGlu3 and mGlu2–mGlu4 heterodimers. Cell Research. 2023;33(10):762-74. doi: 10.1038/s41422-023-00830-2.

60. Yuan Y, Jia G, Wu C, Wang W, Cheng L, Li Q, et al. Structures of signaling complexes of lipid receptors S1PR1 and S1PR5 reveal mechanisms of activation and drug recognition. Cell Research. 2021;31(12):1263-74. doi: 10.1038/s41422-021-00566-x.

61. Kim S, Bielawski J, Yang H, Kong Y, Zhou B, Li J. Functional antagonism of sphingosine-1-phosphate receptor 1 prevents cuprizone-induced demyelination. Glia. 2018;66(3):654-69. Epub 2017/12/02. doi: 10.1002/glia.23272. PubMed PMID: 29193293; PubMed Central PMCID: PMC5773114.

62. Muroi T, Matsushima Y, Kanamori R, Inoue H, Fujii W, Yogo K. GPR62 constitutively activates cAMP signaling but is dispensable for male fertility in mice.

Reproduction. 2017;154(6):755-64. Epub 2017/09/16. doi: 10.1530/rep-17-0333. PubMed PMID: 28912303.

63. Coppi E, Cellai L, Maraula G, Dettori I, Melani A, Pugliese AM, et al. Role of adenosine in oligodendrocyte precursor maturation. Frontiers in Cellular Neuroscience. 2015;9(155). doi: 10.3389/fncel.2015.00155.

64. Shiga H, Asou H, Ito E. Advancement of differentiation of oligodendrocyte progenitor cells by a cascade including protein kinase A and cyclic AMP-response element binding protein. Neurosci Res. 2005;53(4):436-41. Epub 2005/10/04. doi: 10.1016/j.neures.2005.09.004. PubMed PMID: 16198437.

65. Vartanian T, Sprinkle TJ, Dawson G, Szuchet S. Oligodendrocyte substratum adhesion modulates expression of adenylate cyclase-linked receptors. Proceedings of the National Academy of Sciences of the United States of America. 1988;85(3):939-43. doi: 10.1073/pnas.85.3.939. PubMed PMID: 2448785.

66. Shiga H, Yamane Y, Kubo M, Sakurai Y, Asou H, Ito E. Differentiation of immature oligodendrocytes is regulated by phosphorylation of cyclic AMP-response element binding protein by a protein kinase C signaling cascade. J Neurosci Res. 2005;80(6):767-76. doi: 10.1002/jnr.20513. PubMed PMID: 15898102.

67. Sato-Bigbee C, DeVries GH. Treatment of oligodendrocytes with antisense deoxyoligonucleotide directed against CREB mRNA: effect on the cyclic AMP-dependent induction of myelin basic protein expression. J Neurosci Res. 1996;46(1):98-107. Epub

1996/10/01. doi: 10.1002/(sici)1097-4547(19961001)46:1<98::aid-jnr12>3.0.co;2-8. PubMed PMID: 8892110.

68. Afshari FS, Chu AK, Sato-Bigbee C. Effect of cyclic AMP on the expression of myelin basic protein species and myelin proteolipid protein in committed oligodendrocytes: differential involvement of the transcription factor CREB. J Neurosci Res. 2001;66(1):37-45. Epub 2001/10/13. doi: 10.1002/jnr.1195. PubMed PMID: 11599000.

69. Clark RE, Jr., Miskimins WK, Miskimins R. Cyclic AMP inducibility of the myelin basic protein gene promoter requires the NF1 site. Int J Dev Neurosci. 2002;20(2):103-11. Epub 2002/05/30. doi: 10.1016/s0736-5748(02)00013-8. PubMed PMID: 12034141.

70. Gravel M, Gao E, Hervouet-Zeiber C, Parsons V, Braun PE. Transcriptional regulation of 2',3'-cyclic nucleotide 3'-phosphodiesterase gene expression by cyclic AMP in C6 cells. J Neurochem. 2000;75(5):1940-50. doi: 10.1046/j.1471-4159.2000.0751940.x. PubMed PMID: 11032883.

71. Vakilzadeh G, Khodagholi F, Ghadiri T, Darvishi M, Ghaemi A, Noorbakhsh F, et al. Protective Effect of a cAMP Analogue on Behavioral Deficits and Neuropathological Changes in Cuprizone Model of Demyelination. Mol Neurobiol. 2015;52(1):130-41. Epub 2014/08/17. doi: 10.1007/s12035-014-8857-8. PubMed PMID: 25128030.

72. Yoshioka A, Shimizu Y, Hirose G, Kitasato H, Pleasure D. Cyclic AMP-elevating agents prevent oligodendroglial excitotoxicity. J Neurochem. 1998;70(6):2416-23. doi: 10.1046/j.1471-4159.1998.70062416.x. PubMed PMID: 9603206.

73. Raible DW, McMorris FA. Induction of oligodendrocyte differentiation by activators of adenylate cyclase. Journal of Neuroscience Research. 1990;27(1):43-6. doi: https://doi.org/10.1002/jnr.490270107.

74. Raible DW, McMorris FA. Oligodendrocyte differentiation and progenitor cell proliferation are independently regulated by cyclic AMP. Journal of Neuroscience Research. 1993;34(3):287-94. doi: https://doi.org/10.1002/jnr.490340305.

75. Ulmer JB, Edwards AM, McMorris FA, Braun PE. Cyclic AMP decreases the phosphorylation state of myelin basic proteins in rat brain cell cultures. J Biol Chem. 1987;262(4):1748-55. PubMed PMID: 2433287.

76. Vartanian T, Dawson G, Soliven B, Nelson DJ, Szuchet S. Phosphorylation of myelin basic protein in intact oligodendrocytes: inhibition by galactosylsphingosine and cyclic AMP. Glia. 1989;2(5):370-9. doi: 10.1002/glia.440020509. PubMed PMID: 2478466.

77. Dawson G, McAtee P. Differential regulation of basic protein phosphorylation by calcium phospholipid and cyclic-AMP-dependent protein kinases. J Cell Biochem. 1989;40(3):261-9. doi: 10.1002/jcb.240400302. PubMed PMID: 2777906.

78. Vartanian T, Szuchet S, Dawson G, Campagnoni AT. Oligodendrocyte Adhesion Activates Protein Kinase C-Mediated Phosphorylation of Myelin Basic Protein. Science. 1986;234(4782):1395-8. doi: doi:10.1126/science.2431483.

79. Hoi KK, Xia W, Wei MM, Ulloa Navas MJ, Garcia Verdugo JM, Nachury MV, et al. Primary cilia control oligodendrocyte precursor cell proliferation in white matter injury via Hedgehog-independent CREB signaling. Cell Rep. 2023;42(10):113272. Epub 20231017. doi: 10.1016/j.celrep.2023.113272. PubMed PMID: 37858465; PubMed Central PMCID: PMC10715572.

80. Mogha A, D'Rozario M, Monk KR. G Protein-Coupled Receptors in Myelinating Glia. Trends in pharmacological sciences. 2016;37(11):977-87. Epub 2016/09/23. doi: 10.1016/j.tips.2016.09.002. PubMed PMID: 27670389.

81. Jean-Charles P-Y, Kaur S, Shenoy SK. G Protein-Coupled Receptor Signaling Through β-Arrestin-Dependent Mechanisms. Journal of cardiovascular pharmacology. 2017;70(3):142-58. doi: 10.1097/FJC.0000000000000482. PubMed PMID: 28328745.

82. Daniele S, Trincavelli ML, Fumagalli M, Zappelli E, Lecca D, Bonfanti E, et al. Does GRK–β arrestin machinery work as a "switch on" for GPR17-mediated activation of intracellular signaling pathways? Cellular Signalling. 2014;26(6):1310-25. doi: https://doi.org/10.1016/j.cellsig.2014.02.016.

83. Ornelas IM, Khandker L, Wahl SE, Hashimoto H, Macklin WB, Wood TL. The mechanistic target of rapamycin pathway downregulates bone morphogenetic protein

signaling to promote oligodendrocyte differentiation. Glia. 2020;68(6):1274-90. Epub 20200106. doi: 10.1002/glia.23776. PubMed PMID: 31904150; PubMed Central PMCID: PMC7368967.

84. Benardais K, Ornelas IM, Fauveau M, Brown TL, Finseth LT, Panic R, et al. p70S6 kinase regulates oligodendrocyte differentiation and is active in remyelinating lesions. Brain Commun. 2022;4(1):fcac025. Epub 20220212. doi: 10.1093/braincomms/fcac025. PubMed PMID: 35224490; PubMed Central PMCID: PMC8864467.

85. Dahl KD, Almeida AR, Hathaway HA, Bourne J, Brown TL, Finseth LT, et al. mTORC2 Loss in Oligodendrocyte Progenitor Cells Results in Regional Hypomyelination in the Central Nervous System. J Neurosci. 2023;43(4):540-58. Epub 20221202. doi: 10.1523/jneurosci.0010-22.2022. PubMed PMID: 36460463; PubMed Central PMCID: PMC9888514.

86. Fyffe-Maricich SL, Karlo JC, Landreth GE, Miller RH. The ERK2 mitogen-activated protein kinase regulates the timing of oligodendrocyte differentiation. J Neurosci. 2011;31(3):843-50. doi: 10.1523/jneurosci.3239-10.2011. PubMed PMID: 21248107; PubMed Central PMCID: PMC3568938.

87. Brown TL, Hashimoto H, Finseth LT, Wood TL, Macklin WB. PAK1 Positively Regulates Oligodendrocyte Morphology and Myelination. J Neurosci. 2021;41(9):1864-77. Epub 20210121. doi: 10.1523/jneurosci.0229-20.2021. PubMed PMID: 33478987; PubMed Central PMCID: PMC7939082.

88. Ishii A, Furusho M, Dupree JL, Bansal R. Role of ERK1/2 MAPK signaling in the maintenance of myelin and axonal integrity in the adult CNS. J Neurosci. 2014;34(48):16031-45. doi: 10.1523/jneurosci.3360-14.2014. PubMed PMID: 25429144; PubMed Central PMCID: PMC4244469.

89. Jeffries MA, Urbanek K, Torres L, Wendell SG, Rubio ME, Fyffe-Maricich SL. ERK1/2 Activation in Preexisting Oligodendrocytes of Adult Mice Drives New Myelin Synthesis and Enhanced CNS Function. J Neurosci. 2016;36(35):9186-200. doi: 10.1523/jneurosci.1444-16.2016. PubMed PMID: 27581459; PubMed Central PMCID: PMC5005725.

90. Ishii A, Fyffe-Maricich SL, Furusho M, Miller RH, Bansal R. ERK1/ERK2 MAPK signaling is required to increase myelin thickness independent of oligodendrocyte differentiation and initiation of myelination. J Neurosci. 2012;32(26):8855-64. doi: 10.1523/jneurosci.0137-12.2012. PubMed PMID: 22745486; PubMed Central PMCID: PMC3521511.

91. Musah AS, Brown TL, Jeffries MA, Shang Q, Hashimoto H, Evangelou AV, et al. Mechanistic Target of Rapamycin Regulates the Oligodendrocyte Cytoskeleton during Myelination. J Neurosci. 2020;40(15):2993-3007. Epub 20200305. doi: 10.1523/jneurosci.1434-18.2020. PubMed PMID: 32139584; PubMed Central PMCID: PMC7141876.

92. Ahrendsen JT, Harlow DE, Finseth LT, Bourne JN, Hickey SP, Gould EA, et al. The Protein Tyrosine Phosphatase Shp2 Regulates Oligodendrocyte Differentiation and Early Myelination and Contributes to Timely Remyelination. J Neurosci. 2018;38(4):787-802. Epub 20171207. doi: 10.1523/jneurosci.2864-16.2017. PubMed PMID: 29217681; PubMed Central PMCID: PMC5783963.

93. Ishii A, Furusho M, Dupree JL, Bansal R. Strength of ERK1/2 MAPK Activation Determines Its Effect on Myelin and Axonal Integrity in the Adult CNS. J Neurosci. 2016;36(24):6471-87. doi: 10.1523/jneurosci.0299-16.2016. PubMed PMID: 27307235; PubMed Central PMCID: PMC5015783.

94. Narayanan SP, Flores AI, Wang F, Macklin WB. Akt signals through the mammalian target of rapamycin pathway to regulate CNS myelination. J Neurosci. 2009;29(21):6860-70. doi: 10.1523/jneurosci.0232-09.2009. PubMed PMID: 19474313; PubMed Central PMCID: PMC2757755.

95. Flores AI, Narayanan SP, Morse EN, Shick HE, Yin X, Kidd G, et al. Constitutively active Akt induces enhanced myelination in the CNS. J Neurosci. 2008;28(28):7174-83. doi: 10.1523/jneurosci.0150-08.2008. PubMed PMID: 18614687; PubMed Central PMCID: PMC4395496.

96. Dimas P, Montani L, Pereira JA, Moreno D, Trötzmüller M, Gerber J, et al. CNS myelination and remyelination depend on fatty acid synthesis by oligodendrocytes. eLife. 2019;8:e44702. doi: 10.7554/eLife.44702.

97. Sastry PS. Lipids of nervous tissue: composition and metabolism. Prog Lipid Res. 1985;24(2):69-176. doi: 10.1016/0163-7827(85)90011-6. PubMed PMID: 3916238.

98. Choi W-S, Xu X, Goruk S, Wang Y, Patel S, Chow M, et al. FABP7 Facilitates Uptake of Docosahexaenoic Acid in Glioblastoma Neural Stem-like Cells. Nutrients. 2021;13(8):2664. PubMed PMID: doi:10.3390/nu13082664.

99. Bernardo A, Giammarco ML, De Nuccio C, Ajmone-Cat MA, Visentin S, De Simone R, et al. Docosahexaenoic acid promotes oligodendrocyte differentiation via PPAR-γ signalling and prevents tumor necrosis factor-α-dependent maturational arrest. Biochimica et Biophysica Acta (BBA) - Molecular and Cell Biology of Lipids. 2017;1862(9):1013-23. doi: https://doi.org/10.1016/j.bbalip.2017.06.014.

100. Alakbarzade V, Hameed A, Quek DQ, Chioza BA, Baple EL, Cazenave-Gassiot A, et al. A partially inactivating mutation in the sodium-dependent lysophosphatidylcholine transporter MFSD2A causes a non-lethal microcephaly syndrome. Nat Genet. 2015;47(7):814-7. Epub 20150525. doi: 10.1038/ng.3313. PubMed PMID: 26005865.

101. Guemez-Gamboa A, Nguyen LN, Yang H, Zaki MS, Kara M, Ben-Omran T, et al. Inactivating mutations in MFSD2A, required for omega-3 fatty acid transport in brain, cause a lethal microcephaly syndrome. Nat Genet. 2015;47(7):809-13. Epub 20150525. doi: 10.1038/ng.3311. PubMed PMID: 26005868; PubMed Central PMCID: PMC4547531.

102. Harel T, Quek DQY, Wong BH, Cazenave-Gassiot A, Wenk MR, Fan H, et al. Homozygous mutation in MFSD2A, encoding a lysolipid transporter for docosahexanoic acid, is associated with microcephaly and hypomyelination. Neurogenetics. 2018;19(4):227-35. Epub 20180724. doi: 10.1007/s10048-018-0556-6. PubMed PMID: 30043326.

103. Hay CM, Jackson S, Mitew S, Scott DJ, Koenning M, Bensen AL, et al. The oligodendrocyte-enriched orphan G protein-coupled receptor Gpr62 is dispensable for central nervous system myelination. Neural Dev. 2021;16(1):6. Epub 20211129. doi: 10.1186/s13064-021-00156-y. PubMed PMID: 34844642; PubMed Central PMCID: PMC8630896.

104. Blakemore WF. Observations on oligodendrocyte degeneration, the resolution of status spongiosus and remyelination in cuprizone intoxication in mice. Journal of Neurocytology. 1972;1(4):413-26. doi: 10.1007/BF01102943.

105. Tagge I, O'Connor A, Chaudhary P, Pollaro J, Berlow Y, Chalupsky M, et al. Spatio-Temporal Patterns of Demyelination and Remyelination in the Cuprizone Mouse Model. PLOS ONE. 2016;11(4):e0152480. doi: 10.1371/journal.pone.0152480.

106. Gharagozloo M, Mace JW, Calabresi PA. Animal models to investigate the effects of inflammation on remyelination in multiple sclerosis. Front Mol Neurosci. 2022;15:995477. Epub 20221103. doi: 10.3389/fnmol.2022.995477. PubMed PMID: 36407761; PubMed Central PMCID: PMC9669474.

107. Lim DA, Alvarez-Buylla A. The Adult Ventricular-Subventricular Zone (V-SVZ) and Olfactory Bulb (OB) Neurogenesis. Cold Spring Harb Perspect Biol. 2016;8(5). Epub 20160502. doi: 10.1101/cshperspect.a018820. PubMed PMID: 27048191; PubMed Central PMCID: PMC4852803.

108. Radecki DZ, Samanta J. Isolation and culture of neural stem cells from adult mouse subventricular zone for genetic and pharmacological treatments with proliferation analysis. STAR Protocols. 2022;3(1):101153. doi: https://doi.org/10.1016/j.xpro.2022.101153.

109. Lourenço T, Paes de Faria J, Bippes CA, Maia J, Lopes-da-Silva JA, Relvas JB, et al. Modulation of oligodendrocyte differentiation and maturation by combined biochemical and mechanical cues. Scientific Reports. 2016;6(1):21563. doi: 10.1038/srep21563.

110. Gensel JC, Schonberg DL, Alexander JK, McTigue DM, Popovich PG. Semi-automated Sholl analysis for quantifying changes in growth and differentiation of neurons and glia. Journal of Neuroscience Methods. 2010;190(1):71-9. doi: https://doi.org/10.1016/j.jneumeth.2010.04.026.

111. Ristanovic D, Milosevic N. Application of modified Sholl analysis to neuronal dendritic arborization of the cat spinal cord. Journal of Neuroscience Methods. 2006;158, 2006, 212-218.

112. Kuhn S, Gritti L, Crooks D, Dombrowski Y. Oligodendrocytes in Development, Myelin Generation and Beyond. Cells. 2019;8(11). Epub 20191112. doi:

10.3390/cells8111424. PubMed PMID: 31726662; PubMed Central PMCID: PMC6912544.

113. Schmidt H, Hahn G, Deco G, Knösche TR. Ephaptic coupling in white matter fibre bundles modulates axonal transmission delays. PLOS Computational Biology. 2021;17(2):e1007858. doi: 10.1371/journal.pcbi.1007858.

114. Pettigrew DB, Crutcher KA. Myelin contributes to the parallel orientation of axonal growth on white matter in vitro. BMC Neuroscience. 2001;2(1):9. doi: 10.1186/1471-2202-2-9.

115. Zou Y, Zhang WF, Liu HY, Li X, Zhang X, Ma XF, et al. Structure and function of the contactin-associated protein family in myelinated axons and their relationship with nerve diseases. Neural Regen Res. 2017;12(9):1551-8. doi: 10.4103/1673-5374.215268. PubMed PMID: 29090003; PubMed Central PMCID: PMC5649478.

116. Rios JC, Melendez-Vasquez CV, Einheber S, Lustig M, Grumet M, Hemperly J, et al. Contactin-associated protein (Caspr) and contactin form a complex that is targeted to the paranodal junctions during myelination. J Neurosci. 2000;20(22):8354-64. doi: 10.1523/jneurosci.20-22-08354.2000. PubMed PMID: 11069942; PubMed Central PMCID: PMC6773165.

117. Martin AL, Steurer MA, Aronstam RS. Constitutive Activity among Orphan Class-A G Protein Coupled Receptors. PLOS ONE. 2015;10(9):e0138463. doi: 10.1371/journal.pone.0138463.

118. Seamon KB, Padgett W, Daly JW. Forskolin: unique diterpene activator of adenylate cyclase in membranes and in intact cells. Proc Natl Acad Sci U S A. 1981;78(6):3363-7. doi: 10.1073/pnas.78.6.3363. PubMed PMID: 6267587; PubMed Central PMCID: PMC319568.

119. Insel PA, Ostrom RS. Forskolin as a tool for examining adenylyl cyclase expression, regulation, and G protein signaling. Cell Mol Neurobiol. 2003;23(3):305-14. doi: 10.1023/a:1023684503883. PubMed PMID: 12825829.

120. Sharifi K, Ebrahimi M, Kagawa Y, Islam A, Tuerxun T, Yasumoto Y, et al. Differential expression and regulatory roles of FABP5 and FABP7 in oligodendrocyte lineage cells. Cell and Tissue Research. 2013;354(3):683-95. doi: 10.1007/s00441-013-1730-7.

121. Noseda R, Guerrero-Valero M, Alberizzi V, Previtali SC, Sherman DL, Palmisano M, et al. Kif13b Regulates PNS and CNS Myelination through the Dlg1 Scaffold. PLOS Biology. 2016;14(4):e1002440. doi: 10.1371/journal.pbio.1002440.

122. Mich JK, Signer RA, Nakada D, Pineda A, Burgess RJ, Vue TY, et al. Prospective identification of functionally distinct stem cells and neurosphere-initiating cells in adult mouse forebrain. Elife. 2014;3:e02669. Epub 2014/05/21. doi: 10.7554/eLife.02669. PubMed PMID: 24843006; PubMed Central PMCID: PMC4038845.

123. Namchaiw P, Wen H, Mayrhofer F, Chechneva O, Biswas S, Deng W. Temporal and partial inhibition of GLI1 in neural stem cells (NSCs) results in the early maturation

of NSC derived oligodendrocytes in vitro. Stem Cell Res Ther. 2019;10(1):272. Epub 2019/08/29. doi: 10.1186/s13287-019-1374-y. PubMed PMID: 31455382; PubMed Central PMCID: PMC6712625.

124. Boggs JM. Myelin basic protein: a multifunctional protein. Cellular and Molecular Life Sciences CMLS. 2006;63(17):1945-61. doi: 10.1007/s00018-006-6094-7.

125. Yamada M, Iwase M, Sasaki B, Suzuki N. The molecular regulation of oligodendrocyte development and CNS myelination by ECM proteins. Frontiers in Cell and Developmental Biology. 2022;10. doi: 10.3389/fcell.2022.952135.

126. Clawson ED, Radecki DZ, Samanta J. Immunofluorescence assay for demyelination, remyelination, and proliferation in an acute cuprizone mouse model. STAR Protocols. 2023;4(1):102072. doi: https://doi.org/10.1016/j.xpro.2023.102072.

Figures created with BioRender.com.

APPENDIX A

Immunofluorescence assay for demyelination, remyelination, and proliferation in an acute cuprizone mouse model

Elizabeth D. Clawson, Daniel Z. Radecki, Jayshree Samanta,

STAR Protocols,

Volume 4, Issue 1, 2023

102072, ISSN 2666-1667

https://doi.org/10.1016/j.xpro.2023.102072.

(https://www.sciencedirect.com/science/article/pii/S2666166723000308)

Abstract

Here, we present a protocol to assess demyelination in the corpus callosum of an acute cuprizone mouse model, which is routinely used to induce demyelination for studying myelin regeneration in the rodent brain. We describe the tracing of neural stem cells via intraperitoneal injection of tamoxifen into adult Gli1^{CreERT2};Ai9 mice and the induction of demyelination with cuprizone diet. We also detail EdU administration, cryosectioning of the mouse brain, EdU labeling, and immunofluorescence staining to examine proliferation and myelination. For complete details on the use and execution of this protocol, please refer to Radecki et al. (2020).

STAR Protocols

CellPress
OPEN ACCESS

Protocol

Immunofluorescence assay for demyelination, remyelination, and proliferation in an acute cuprizone mouse model

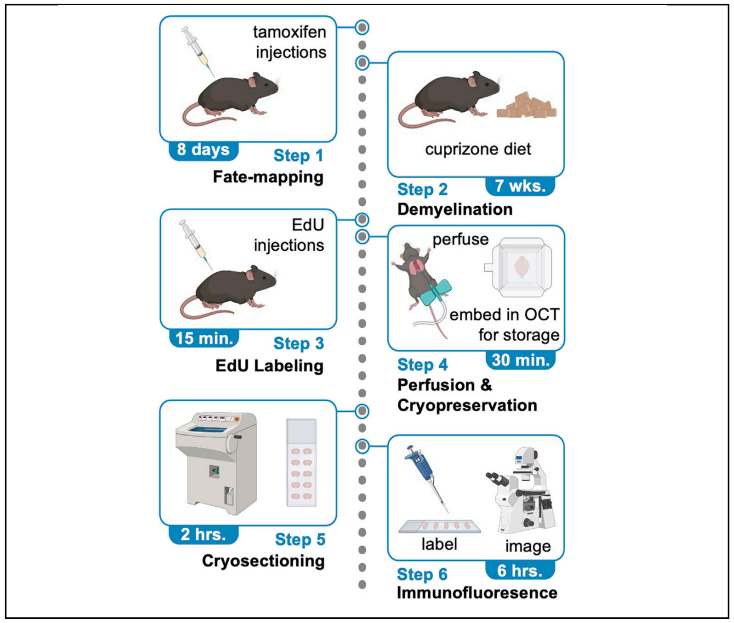

Here, we present a protocol to assess demyelination in the corpus callosum of an acute cuprizone mouse model, which is routinely used to induce demyelination for studying myelin regeneration in the rodent brain. We describe the tracing of neural stem cells via intraperitoneal injection of tamoxifen into adult Gli1CreERT2;Ai9 mice and the induction of demyelination with cuprizone diet. We also detail EdU administration, cryosectioning of the mouse brain, EdU labeling, and immunofluorescence staining to examine proliferation and myelination.

Publisher's note: Undertaking any experimental protocol requires adherence to local institutional guidelines for laboratory safety and ethics.

Elizabeth D. Clawson, Daniel Z. Radecki, Jayshree Samanta

elizabeth.clawson@wisc.edu (E.D.C.)
jayshree.samanta@wisc.edu (J.S.)

Highlights

Administering tamoxifen for lineage tracing and EdU for labeling proliferating cells

Inducing demyelination in adult mice with cuprizone diet

Harvesting and cryosectioning the brain

Detecting proliferation with EdU labeling and demyelination with immunofluorescence

Clawson et al., STAR Protocols 4, 102072
March 17, 2023
https://doi.org/10.1016/j.xpro.2023.102072

STAR Protocols

CellPress
OPEN ACCESS

Protocol

Immunofluorescence assay for demyelination, remyelination, and proliferation in an acute cuprizone mouse model

Elizabeth D. Clawson,[1,2,3,4,*] Daniel Z. Radecki,[1,3] and Jayshree Samanta[1,2,3,5,*]

[1]Department of Comparative Biosciences, University of Wisconsin-Madison, Madison, WI 53706, USA

[2]Molecular and Cellular Pharmacology Program, University of Wisconsin-Madison, Madison, WI 53706, USA

[3]Stem Cell and Regenerative Medicine Center, University of Wisconsin-Madison, Madison, WI 53706, USA

[4]Technical contact

[5]Lead contact

*Correspondence: elizabeth.clawson@wisc.edu (E.D.C.), jayshree.samanta@wisc.edu (J.S.)
https://doi.org/10.1016/j.xpro.2023.102072

SUMMARY

Here, we present a protocol to assess demyelination in the corpus callosum of an acute cuprizone mouse model, which is routinely used to induce demyelination for studying myelin regeneration in the rodent brain. We describe the tracing of neural stem cells via intraperitoneal injection of tamoxifen into adult Gli1CreERT2;Ai9 mice and the induction of demyelination with cuprizone diet. We also detail EdU administration, cryosectioning of the mouse brain, EdU labeling, and immunofluorescence staining to examine proliferation and myelination. For complete details on the use and execution of this protocol, please refer to Radecki et al. (2020).[1]

BEFORE YOU BEGIN

Breed the Gli1$^{CreERT2/CreERT2}$ mice with Ai9$^{Fx/Fx}$ reporter mice to generate Gli1$^{CreERT2/WT}$;Ai9$^{Fx/WT}$ (Gli1^{CreERT2};Ai9) mice. In these mice, intraperitoneal administration of Tamoxifen to 8–12 week old male or female mice permanently labels the Gli1 expressing cells with tdTomato. The Gli1^{CreERT2} mice have CreERT2 knocked into the Gli1 locus such that the homozygous mice lack all Gli1 expression but are viable and fertile. In the Ai9 mice, a CAG promoter driving TdTomato fluorescent protein is inserted into the Gt(ROSA)26Sor locus. A *loxP*-flanked stop cassette prevents transcription of TdTomato in the absence of Tamoxifen. This protocol describes the steps for inducing demyelination with cuprizone diet, and harvesting the brain after intracardiac perfusion with paraformaldehyde, followed by cryosectioning of the brains for immunofluorescent staining to detect demyelination and remyelination, and EdU labeling to detect proliferation.

Institutional permissions

The use of mice in this protocol was approved and performed according to the regulations of the University of Wisconsin-Madison's Institutional Animal Care and Use Committee. Before beginning, approval must be obtained from each researcher's own institution.

Preparation for cuprizone diet and tamoxifen and EdU injections

Timing: 2–4 weeks

1. Order 0.2% Cuprizone diet in non-irradiated pelleted form, packaged in 1 kg vacuum sealed bags, at least 2 weeks prior to starting the experiment to ensure sufficient time for delivery.

Note: Store the unopened Cuprizone diet bags at −20°C until the expiration date on the package, which is usually 6 months from the manufacturing date. Refrigerate the opened bags at 4°C, and use within 4 weeks.

2. Prepare 20 mg/mL Tamoxifen solution.
   a. Dissolve 100 mg of Tamoxifen into 5 mL corn oil in a 50 mL conical tube.
   b. Shake for 4–6 h at 250 rpm in a 37°C incubator until the solution is clear and all the particles have dissolved.

Note: Keeping the solution at 37°C for extended periods may degrade the drug.

⚠ CRITICAL: Store Tamoxifen at −20°C in the powder form until the expiration date on the vial. After dissolving in corn oil, store the Tamoxifen solution at 4°C for a maximum period of four weeks.

3. Prepare 25 mg/mL EdU (5-ethynyl-2′-deoxyuridine) stock solution.
   a. Dissolve 250 mg EdU in 10 mL DMSO by vigorous mixing on a vortex mixer.
   b. Make 1 mL aliquots in microfuge tubes and store at −80°C until the manufacturer's expiration date.

Note: Store EdU at −80°C in the powdered form until the expiration date on the vial.

KEY RESOURCES TABLE

REAGENT or RESOURCE	SOURCE	IDENTIFIER
Antibodies		
Mouse IgG2b anti-APC (CC-1), (1:100)	Thermo Fisher Scientific	Cat# OP80, RRID: AB_2057371
Rabbit anti-NG2, (1:200)	Sigma-Aldrich	Cat# AB5320, RRID: AB_2314937
Rat anti-RFP, (1:1000)	ChromoTek	Cat# 5F8-100, RRID: AB_2336064
Mouse IgG2b anti-MBP (SMI99), (1:100)	BioLegend	Cat# 808402, RRID: AB_2564742
Alexafluor Goat anti-Rabbit 568, (1:1000)	Thermo Fisher Scientific	Cat# A11011, RRID: AB_143157
Alexafluor Goat anti-mouse IgG2b 488, (1:1000)	Thermo Fisher Scientific	Cat# A21141, RRID: AB_2535778
Alexafluor Goat anti-rat 568, (1:1000)	Thermo Fisher Scientific	Cat# A48262, RRID: AB_2896330
Chemicals, peptides, and recombinant proteins		
32% paraformaldehyde solution	EMS	Cat# 15714-S
FatalPlus (390 mg/mL pentobarbitol sodium solution) euthanasia	Vortech Pharmaceuticals	V.P.L. 9373 N.D.C. No. 0298-9373-68
Tamoxifen	Cayman Chemical	Cat# 13258
Corn oil	Sigma-Aldrich	Cat# C8267-500mL
Goat serum	Thermo Fisher Scientific	Cat# 10000C
EdU (5-ethynyl-2′-deoxyuridine)	Cayman Chemical	Cat# 20518
10× phosphate buffered aaline (PBS)	IBI Scientific	Cat# IB70165
Bovine serum albumin (BSA)	Thermo Fisher Scientific	Cat# BP9703-100
Triton X-100	Thermo Fisher Scientific	Cat# 85111
Sucrose	Dot Scientific	Cat# DSS24060
Hoechst 33258	Thermo Fisher Scientific	Cat# H3569
Fluoromount-G	Southern Biotech	Cat# 0100-01
2016, Teklad Global 16% Protein Rodent Diet with 0.2% Cuprizone [bis(cyclohexane)oxaldihydrazone]	Envigo	TD.140800
Covergrip Coverslip Sealant	Biotium	Cat# 23005
Critical commercial assays		
Click-iT Plus EdU Alexa Fluor 647 Imaging Kit	Thermo Fisher Scientific	Cat# C10640

(*Continued on next page*)

Continued		
REAGENT or RESOURCE	SOURCE	IDENTIFIER
Experimental models: Organisms/strains		
Gli1^{CreERT2} Mouse: strain-C57bl/6J, genotype- *Gli1*$^{CreERT2/+}$, sex- Male or Female, Age- 8 to 10 weeks	The Jackson Laboratory	Stock# 007913, *Gli1*$^{tm3(cre/ERT2)Alj}$/J
Ai9^{FX} Mouse: strain-C57bl/6J, genotype- Ai9$^{FX/FX}$, sex- Male or Female, Age- 8 to 10 weeks	The Jackson Laboratory	Stock# 007909, *ROSA26Sor*$^{tm9(CAG-tdTomato)Hze}$
Software and algorithms		
GraphPad Prism	Dotmatics	https://www.graphpad.com/scientific-software/prism/
NIH ImageJ Fiji	Schindelin et al.[2]	https://imagej.net/software/fiji/
Other		
Gilson MINIPULS 3 peristaltic pump	Gilson	Cat# F155001
Vortex mixer	Gilson	Cat# 36110740
1 oz feeding jar set (individual mouse) (alternate for powdered diet)	Dyets Inc	Cat# 910019
Cuprizone (alternate for powdered diet)	Sigma-Aldrich	Cat# C9012-25G
50 mL conical polypropylene tubes	Celltreat	Cat# 229421
Cork board for dissection	VWR	Cat# 100498-390
Scalp vein set butterfly 27G	VWR	Cat# MSPP-EXL-26709
Nalgene 3-way Stopcock	Thermo Fisher Scientific	Cat# 6470-0002
Std pattern tissue forceps	Braintree Scientific	Cat# FC1 10
Supercut iris scissors, straight	Braintree Scientific	Cat# SCT-I 528
SuperCut surgical scissors, curved	Braintree Scientific	Cat# SCT-S 511
Std pattern dressing forceps	Braintree Scientific	Cat# FC100 2
Dumont forceps	Braintree Scientific	Cat# FC-5043
Flat blade membrane forceps	Thermo Fisher Scientific	Cat# 09-753-50
Fluoromount-G	Southern Biotech	Cat# 0100-01
Superfrost Plus Microscope Slides	Thermo Fisher Scientific	Cat# 12-550-15
Nutating mixer	Midwest Scientific	Cat# NS-10A
Tissue-Tek OCT media	Sakura	Cat# 4583
Peel-A-Way Embedding Molds (Square-S22)	Polysciences, Inc.	Cat# 1864A-1
Kimwipes disposable wipes	Millipore Sigma	Cat# Z188956
Tissue-Tek Accu-Edge Low Profile blades (tissue slicer blades)	Sakura	Cat# 4685
Cryostat	Leica	Cat# CM3050 S
Golden nylon brushes for cryo microtomy	Ted Pella	Cat# 11842A
A-PAP pen	Ted Pella	Cat# 22309
Gauze sponges	Thermo Fisher	Cat# 22-362178
Tuberculin syringe with 28G needle	BD Biosciences	Cat# 329461
22 × 50 mm glass coverslip	Corning	Cat# 2975-225
Precision glide needles 16G	BD Biosciences	Cat# 305198
Precision glide needles 27G	BD Biosciences	Cat# 305109
Fluorescent ,icroscope	Keyence	Cat# BZ-X710
Confocal microscope	Leica	Cat# SP8

MATERIALS AND EQUIPMENT

20 mg/mL tamoxifen solution		
Reagent	Final concentration	Amount
Tamoxifen	20 mg/mL	100 mg
Corn oil	N/A	5 mL
Total	**N/A**	**5 mL**

Note: Store Tamoxifen solution at 4°C for up to four weeks.

⚠ CRITICAL: Tamoxifen is a carcinogen and teratogen. Weigh the tamoxifen powder inside a fume hood. Use appropriate PPE consisting of nitrile gloves, surgical mask, safety goggles and lab coat while handling tamoxifen.

4% paraformaldehyde solution		
Reagent	Final concentration	Amount
32% paraformaldehyde (PFA)	4%	4.4 mL
10× PBS	1× PBS	3.5 mL
Distilled water	N/A	27.1 mL
Total	**N/A**	**35 mL**

Note: Prepare fresh for each set of perfusions or store at 4°C and use within 24 h.

⚠ CRITICAL: PFA is a suspected carcinogen and an irritant. Perform all perfusions in a fume hood and use appropriate PPE consisting of nitrile gloves, surgical mask, safety goggles and lab coat while handling PFA.

30% sucrose solution		
Reagent	Final concentration	Amount
sucrose	30%	30 g
10× PBS	1×	10 mL
Distilled water	N/A	90 mL
Total	**N/A**	**100 mL**

Note: Store sucrose solution at 4°C for up to 6 months. However, discard the solution if cotton ball like fungal growth is observed before 6 months.

BSA-Triton X-100 solution		
Reagent	Final concentration	Amount
Bovine Serum Albumin	0.1%	0.1 g
Triton X-100	0.25%	25 µL
10× PBS	1×	1 mL
Distilled water	N/A	8.975 mL
Total	**N/A**	**10 mL**

Note: Prepare fresh and keep on ice or store at 4°C and use within 24 h.

Blocking buffer		
Reagent	Final concentration	Amount
Normal goat serum	10%	50 µL
BSA-Triton X-100 solution	N/A	450 µL
Total	**N/A**	**500 µL**

Note: Prepare fresh and keep on ice or store at 4°C to be used within 24 h.

PBS-Triton X-100 solution		
Reagent	Final concentration	Amount
10% Triton X-100	0.5%	500 μL
10× PBS	1×	1 mL
Distilled water	N/A	8.5 mL
Total	**N/A**	**10 mL**

Note: Store at room temperature for up to two months.

3% BSA-PBS solution		
Reagent	Final concentration	Amount
Bovine Serum Albumin	3%	0.3 g
10× PBS	1×	1 mL
Distilled water	N/A	9 mL
Total	**N/A**	**10 mL**

Note: Make fresh and keep on ice or store at 4°C and use within 24 h.

EdU stock solution		
Reagent	Final concentration	Amount
EdU	25 mg/mL	250 mg
DMSO	N/A	10 mL
Total	**N/A**	**10 mL**

Note: Make 1 mL aliquots and store at −80°C for a year. Avoid repeated freeze thaw cycles.

EdU working solution		
Reagent	Final concentration	Amount
EdU stock solution (25 mg/mL)	2.5 mg/mL	1 mL
10× PBS	1×	1 mL
Distilled water	N/A	8 mL
Total	**N/A**	**10 mL**

Note: Prepare fresh and use within 2 h at room temperature.

Alternatives: Substitute PBS with Hanks Balanced Salt Solution (HBSS) or 0.9% Saline.

1× Click-iT EdU reaction buffer		
Reagent	Final concentration	Amount
Component D in Click-iT EdU imaging kit	1×	4 mL
Deionized water	N/A	36 mL
Total	**N/A**	**40 mL**

Note: Store at 4°C for 6 months.

10× Click-iT EdU buffer additive		
Reagent	Final concentration	Amount
Component F in Click-iT EdU imaging kit	10×	400 mg
Deionized water	N/A	2 mL
Total	**N/A**	2 mL

Note: Store at ≤20°C for one year. Discard if the solution develops a brown color.

1× Click-iT EdU buffer additive		
Reagent	Final concentration	Amount
10× Click-iT EdU buffer additive	1×	5 µL
Deionized water	N/A	45 µL
Total	**N/A**	50 µL

Note: Prepare fresh and keep on ice or store at 4°C and use within 24 h.

Click-iT Plus reaction cocktail (add the reagents in the order below for one slide):		
Reagent	Final concentration	Amount
1× Click-iT EdU reaction buffer	N/A	440 µL
copper protectant (component E)	N/A	10 µL
Alexa Fluor picolyl azide (component B)	N/A	1.2 µL
1× Click-iT EdU buffer additive	0.1×	50 µL
Total	**N/A**	501.2 µL

Note: Prepare fresh and use within 15 min at room temperature (20°C–25°C).

STEP-BY-STEP METHOD DETAILS

Administration of cuprizone, tamoxifen, and EdU

Timing: 7 weeks

In this step, the Gli1 expressing cells are fate-mapped by intraperitoneal administration of Tamoxifen to Gli1CreERT2;Ai9 mice and demyelination is induced 1 week later by feeding 0.2% cuprizone diet for 5 weeks. In addition, the proliferating cells are labeled by intraperitoneal administration of EdU a day prior to euthanasia.

1. Inject 5 mg tamoxifen per day intraperitoneally on alternate days for 4 injections (total 20 mg/mouse).
   a. Fill the 1 mL tuberculin syringe with Tamoxifen and wipe the tip of the filled syringe with a kimwipe, before attaching a 27G needle to the syringe.
   b. Administer 250 µL/day (5 mg/day) of 20 mg/mL Tamoxifen by intraperitoneal (i.p.) injection to each mouse, on alternate days, for a total of 4 i.p. injections.
      i. Scruff the mouse and insert the needle into the lower left or right quadrant of the abdomen, perpendicular to the surface of the skin.
      ii. After insertion, aspirate to check for the presence of fluid prior to injecting the drug.
      iii. Alternate between the left and right side for i.p. injections.

STAR Protocols
Protocol

⚠ CRITICAL: Ideally there should not be any fluid aspirate before injecting the drug. If a blood vessel is punctured by the needle, the aspirated fluid will be red blood and if the urinary bladder is punctured by the needle, the aspirated fluid will be clear or yellow urine. Injecting Tamoxifen into the bladder can lead to urinary tract inflammation and death if not treated promptly. In case fluid is aspirated, remove and discard the needle properly. Using a clean syringe, perform the i.p. injection again at a different site. If the bladder is punctured, watch for turbid white discharge from the urethra for about 2 days, which indicates a urinary tract infection.

Note: The typical dose of Tamoxifen is 100 mg/kg live weight. However, we examined the recombination efficiency with i.p. injections of 1–6 mg/day tamoxifen on 4 alternate days and found that 20 mg Tamoxifen ensures recombination of the floxed allele in adult mice of C57bl/6 and swiss webster background strains with weights ranging from 20 g to 60 g, without any toxic effects on neural stem cells. We have also used this dosage in multiple CreER and floxed mouse lines.[1,3,4]

2. One week after the last Tamoxifen injection, change the diet to 0.2% cuprizone pellets.
   a. Transfer the mice to a clean cage before starting cuprizone diet to prevent the mice from eating any leftover regular chow buried in the bedding.
   b. Provide the cuprizone diet and water ad libitum for 5 weeks.
      i. Discard the pellets in the cage, every 2–3 days and replenish with fresh cuprizone pellets, since the drug degrades gradually with time.

⚠ CRITICAL: Feeding 3 g per mouse per day is sufficient to avoid discarding excessive amounts of food.

   c. After 5 weeks of cuprizone diet, change the diet to regular chow to allow for remyelination.

Note: Analyze remyelination from 2–10 weeks after cessation of cuprizone diet.

Note: Store the vacuum sealed bags of Cuprizone pellets at −20°C. Refrigerate the opened bag at 4°C, away from light and use within 4 weeks.

Alternatives: Instead of the pellets, provide 0.2% Cuprizone diet in the powdered form by mixing 0.2 g of cuprizone with 99.8 g of powdered chow. For the healthy control mice, feed regular chow in the powdered form. Place the powdered diet in a feeding jar on the floor of the cage and change the diet every day to minimize consumption of food contaminated with urine and feces.

3. Administer EdU by i.p. injection, 24 h prior to euthanasia.
   a. Prepare working solution of EdU (2.5 mg/mL).
   b. Administer 20 µL of 2.5 mg/mL working solution per gram body weight of mouse, or 50 mg/kg body weight, by a single i.p. injection following the precautions mentioned in step 1.

Intracardiac perfusion and harvesting the brain

Timing: 30 min per mouse

In this step, Gli1CreERT2;Ai9 mice are perfused by intracardiac administration of 4% Paraformaldehyde (PFA) and their brains are cryopreserved by embedding in OCT.

4. Set up the peristaltic pump.
   a. Connect the scalp vein set tubing to the outlet tube of the peristaltic pump.

b. Insert one tube of the pump into a container with 1× PBS (30 mL/mouse) and another tube into a container with 4% PFA solution (30 mL/mouse).
c. Attach the tubing from the two containers to a 3-way stopcock.
d. Set the pump speed at 8 mL/min and fill the main outlet line with 1× PBS until there is a steady stream without bubbles from the needle.
e. Turn off the peristaltic pump and turn the stopcock to allow the flow of 4% PFA.
f. Pump 4% PFA until the fluid has reached the stopcock but not entered the main line.
g. Turn off the peristaltic pump and turn the stopcock to allow the flow of 1× PBS.

5. Anesthetize the mouse.
   a. Administer 120 mg/kg of Fatal Plus (390 mg/mL Pentobarbitol sodium), via i.p. injection using a tuberculin syringe with 27G needle.

   ⚠ CRITICAL: Fatal-Plus is a controlled substance. A DEA license is required to purchase it.

   b. Lay the mouse on its back on a cork board or a flat piece of styrofoam placed in a dissecting tray, after the mouse is completely unresponsive to painful stimuli, such as a sharp toe pinch, but the heart is still beating.
   c. Pin all four limbs of the mouse to the cork board using dissection pins or needles.
6. Expose the heart.
   a. Incise the skin over the abdomen and chest with a large forcep (std. pattern tissue forceps) and dissecting scissors (supercut surgical scissors).
   b. Incise the diaphragm with small dissecting scissors (supercut iris scissor), being careful not to puncture the beating heart.
   c. Cut the ribcage on both sides of the sternum with a small scissor (supercut iris scissor).
   d. Lift the sternum with a forcep (std. pattern dressing forceps) to expose the heart.
   e. Pin the xiphoid process of the overturned sternum to the dissection board with a needle.
7. Intracardiac perfusion.
   a. Gently lift off the white membrane like thymus covering the upper part of the heart with a forcep (std. pattern dressing forceps).
   b. Make a nick in the right auricle which is the dark appendage attached to the right atrium, using the tip of small pointed scissors (supercut iris scissor) (Figure 1A).

   Note: This allows the blood and perfusion fluids to drain into the dissection tray.

   c. Insert the butterfly needle, connected to the main line of the peristaltic pump, into the apex of the heart, which is formed by the left ventricle (Figure 1A).
   d. Turn on the peristaltic pump and perfuse with 30 mL of 1× PBS at approximately 8 mL/min.
   e. Switch the stopcock to perfuse with 30 mL of 4% PFA at the same rate.

   Note: Curling and stiffening of the tail is the earliest indication of a good perfusion. Subsequently the liver becomes pale and the body stiffens when perfused well. (See troubleshooting Problem 1) Ideally, the lungs should not inflate and fluid should not ooze out of the nose or mouth during perfusion. (See troubleshooting Problem 2).

   ⚠ CRITICAL: If bubbles appear in the main line, remove the needle from the heart to expel the bubble and reinsert it into the heart.

8. Collect the brain.
   a. Remove the needle from the heart and the pins holding the mouse to the dissection board.
   b. Cut the head at the base of the skull with large scissors (supercut surgical scissors) (Figure 1Bi).

STAR Protocols
Protocol

CellPress
OPEN ACCESS

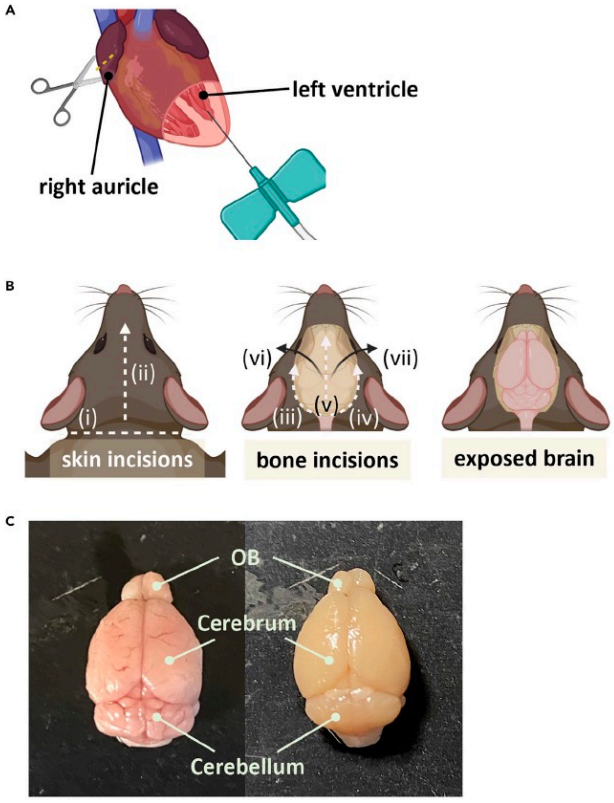

Figure 1. Perfusion and brain harvest

(A) Illustration of the incision point for creating an outlet for the blood and perfusion fluids, and the insertion point for the butterfly needle, demonstrating the position of the needle in the left ventricle.

(B) Illustration of mouse brain harvest. Incisions for separating the skin (i-ii), and the bone (iii-vii) to expose the brain.

(C) Examples of incompletely perfused (left) vs. completely perfused brains (right).

c. Remove the skin from the dorsal side of the head (Figure 1Bii) using a smaller pair of scissors (supercut iris scissor).

d. Insert the blade of a small scissor (supercut iris scissor) through the foramen magnum and cut the skull bone laterally up to the orbit on both sides, taking care not to nick the brain (Figure 1Biii-iv).

e. Make another midline incision through the skull bone, along the sagittal suture, anteriorly past the eyes with a small scissor (supercut iris scissor) (Figure 1Bv).

f. Carefully remove the skull bone from around the brain using a pair of thin pointed forceps (Dumont forceps), starting by gently pulling the bone laterally, away from the midline on either side (Figure 1Bvi-vii).

g. When reaching the area of the skull encasing the olfactory bulbs, it may be necessary to make a few more small snips to release the olfactory bulbs.

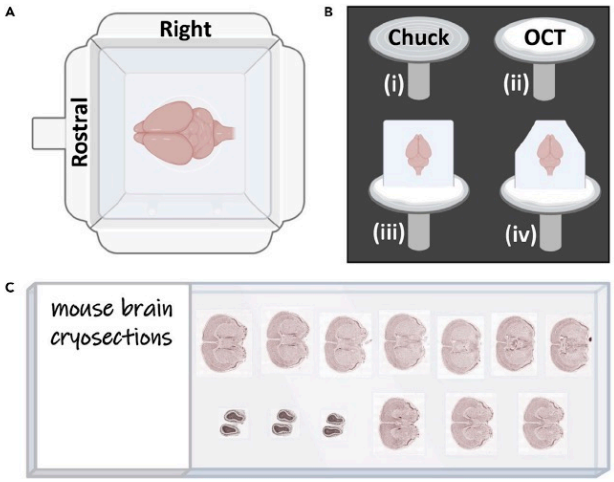

Figure 2. Cryopreservation and cryosectioning

(A) Illustration of the brain embedded in OCT in a tissue mold.

(B) Illustration of mounting the frozen tissue block for cryosectioning coronal sections. The chuck is coated with a layer of OCT (i-ii), and the frozen tissue block firmly pressed into the OCT on the chuck (iii). Excess OCT can be carefully trimmed before sectioning (iv).

(C) Illustration of olfactory bulb and forebrain sections (from Allen Brain Atlas) on a slide.

Note: Ensure that the olfactory bulbs are no longer attached to the bone before removing the brain.

h. Separate the brain along with the olfactory bulbs from the skull using a pair of flat forceps (flat blade membrane forceps), and drop it into a 15 mL conical tube containing 5 mL of 4% PFA.

Note: A well-perfused brain appears pale and does not have a pinkish or red color (Figure 1C) (See troubleshooting Problem 3).

i. Incubate the brain in 4% PFA for 4–6 h at 4°C.

9. Cryoprotect the brain.

a. Gently remove the brain from the 4% PFA solution by emptying the tube in a petri dish.

b. Drop the brain into a 15 mL conical tube containing 15 mL of 30% sucrose solution using flat forceps (flat blade membrane forceps).

Note: The brain should float to the top of the solution.

c. Incubate at 4°C on a nutating mixer at 20–30 rpm, overnight for 12–16 h.

Note: After incubation, the brain should be at the bottom of the tube due to increase in density.

⚠ CRITICAL: Minimize the amount of air space in the tube containing 30% sucrose to ensure that the brain remains submerged in the solution and the surface does not dry.

Pause point: Brains can be incubated in 30% sucrose solution for up to 24 h at 4°C.

10. Embed brains in OCT media and freeze.
    a. Label the tissue mold and add OCT media into the mold.
    b. Remove the brain from sucrose solution by gently emptying the tube into a petri dish.
    c. Pick the brain with flat forceps (flat blade membrane forceps) and roll it on lint free paper napkin like kimwipe to remove the excess sucrose from the surface.
    d. With minimal pressure, gently lift the brain with flat forceps (flat blade membrane forceps) and place it into the mold with the ventral surface facing the bottom of the mold (Figure 2A).

Note: Add more OCT on top if needed, to submerge the brain completely in OCT.

    e. Immediately place the mold on a level surface in the −80°C freezer for at least 24 h prior to cryosectioning.

Pause point: Brains can be stored in OCT at −80°C for years.

Cryosectioning

Timing: 3 h per brain for beginners

In this step, the brain is sectioned into 20 μM thick sections.

11. Equilibrate the temperature of the embedded frozen brain to that of the cryostat by incubating the brain at −20°C, either in a freezer or in the cryostat, at least 1 h prior to sectioning.

Pause point: The frozen brain can be kept in a −20°C freezer for 12–16 h before sectioning.

12. Place a fresh cryostat blade, a 25 mm diameter metal specimen holder or chuck, and a brush inside the cryostat, at least 30 min prior to sectioning, to equilibrate their temperature to −20°C.
13. Mount the brain to the specimen holder or chuck.
    a. Remove the plastic mold from the embedded brain by cutting the 4 corners with a razor or a used cryostat blade.
    b. Pour OCT medium on the pre-cooled chuck (Figure 2Bi) inside the cryostat; quantity should be enough to cover the surface (~500 μL) (Figure 2Bii).
    c. Immediately place the embedded brain on the OCT before it freezes (Figure 2Biii).

Note: For coronal sections, position the brain so that the caudal end is facing the chuck and the rostral end is facing you. For sagittal sections, place the brain on its side.

    d. Allow the brain to freeze on the chuck for 10–20 min before sectioning.
14. Collect 20 μM sections of the brain.
    a. Clamp the chuck firmly into the object head of the cryostat.
    b. Turn on the cryostat and trim the block until the brain tissue is visible.
    c. Trim the excess OCT from the sides of the block with a razor or a used cryostat blade (Figure 2Biv).
    d. Collect about 3–5 sections of the olfactory bulb and 8–10 sections of the forebrain, starting from the genu of the corpus callosum to the hippocampal commissure, on each slide (Figure 2C).

⚠ CRITICAL: To avoid wrinkling of the tissue section, apply a drop of PBS on the slide with a brush and immediately collect the section on the PBS.

(See troubleshooting Problem 4).

(See troubleshooting Problem 5).

Note: Use a gauze sponge dipped in PBS to remove unwanted tissue sections and OCT from the slide. To avoid detachment of the section from the slide in subsequent procedures like immunohistochemistry, prevent OCT from collecting between the tissue and the surface of the slide (Figure 2C).

15. To dry the sections, keep the slides on a flat surface at room temperature, overnight or for 12–16 h.
16. After drying, keep the slides in a slide storage box at −80°C.

Pause point: The cryosections on the slides can be stored at −80°C for years.

Immunofluorescent staining and EdU labeling

Timing: 18–22 h

In this step, EdU labeling is followed by immunofluorescence of the brain cryosections to examine proliferation and myelination respectively.

17. Equilibrate the frozen slides to room temperature for at least 15 min.
    a. Place the slides in a moist chamber prepared with a paper towel soaked in distilled water in a tray.

    Note: Balance the slides on two rods or serological pipets glued/taped to the tray (Figure 3A).

    b. Draw a line with a PAP pen along the periphery of the slide to form a hydrophobic barrier for minimizing the amount of reagents used per slide.

    Note: If needed, gently wipe the condensation on the edge of the slide without touching the cryosections, with a kimwipe before using the pap pen.

    c. After 15 min, wash the sections once with 500–800 µL 1 × PBS for 5 min at room temperature (20°C–25°C).
    d. After the wash, remove the PBS either by tilting the slide to pour the liquid into the tray or aspirate the liquid with vacuum suction (Figure 3B).

    Note: To prevent the cryosections from lifting off the slide during suctioning, attach a 200 µL pipet tip to the tip of the glass pipette attached to the suction tube for slowing the aspiration (Figure 4B).

18. EdU labeling with Click-iT Plus EdU imaging kit.

    Note: EdU labelling kits are available for many wavelengths depending on the microscope filter or laser used for imaging. We have used the Click-iT Plus Alexa-647 kit. The following steps are modified from the manufacturer's directions in Life Technologies MAN0009885 MP10637 Revision A.0.

    a. Add 500 µL of 0.5% PBS-Triton X-100 solution on each slide to permeabilize the tissue.
    b. Incubate for 20 min at room temperature (20°C–25°C).
    c. Meanwhile, prepare the 1 × Click-iT EdU buffer additive and use it to prepare the Click-iT Plus reaction cocktail.

d. Remove the PBS-Triton X-100 and wash the slide twice with 3% BSA-PBS solution.
e. Add 500 µL Click-iT Plus reaction cocktail to the slide and incubate for 30 min at room temperature (20°C–25°C).

Note: Protect from light by covering the transparent lid of the tray with aluminum foil.

⚠ CRITICAL: From this point onward, protect the tissue from light in all the steps.

f. Remove the Click-iT Plus reaction cocktail and wash once with 3% BSA-PBS solution for 5 min at room temperature (20°C–25°C).
g. Remove the 3% BSA-PBS solution.
h. Wash 3 times with 500–800 µL of 1× PBS for 10 min each at room temperature (20°C–25°C) before continuing with immunofluorescence.

19. Immunofluorescence.
a. **Optional**: This step is specifically needed for immunofluorescence of Myelin Basic Protein (MBP). For all other proteins, you can start from step 19c.
i. Fix the tissue with methanol to enhance detection of myelin proteins by adding 500 µL of cold methanol (stored at −20°C) on each slide.
ii. Incubate at room temperature (20°C–25°C) for 15 min (See troubleshooting Problem 6).
iii. Remove the methanol.
iv. Wash the slide 3 times with 500–800 µL of 1× PBS per slide for 10 min/wash at room temperature (20°C–25°C).
b. To minimize non-specific binding of the primary antibody to the tissue, add 500 µL of blocking buffer per slide.
c. Incubate for 45 min to 1 h at room temperature (20°C–25°C).
d. Remove the blocking solution.
e. Add 500 µL of primary antibody per slide.

Note: Dilute the primary antibody in the BSA-Triton X100 solution to obtain the desired concentration.

f. Incubate with the primary antibody for 2 h at room temperature (20°C–25°C) or overnight at 4°C.

⏸ **Pause point:** Slides can be incubated in primary antibody for up to 24 h at 4°C.

g. Remove the primary antibody.
h. Wash 3 times with 500–800 µL of 1× PBS per slide for 10 min/wash at room temperature.
i. Remove the PBS.
j. Add 500 µL of the secondary antibody with Hoechst stain per slide.

Note: Dilute the Alexafluor secondary antibodies 1:1000 fold and the Hoechst nuclear stain 1:5000 fold in the BSA-Triton X100 solution.

k. Incubate with the secondary antibody plus Hoechst for 1 h at room temperature (20°C–25°C), protected from light.

Note: We do not recommend longer incubation periods since they can result in higher background staining.

⚠ CRITICAL: For performing immunofluorescence without EdU labelling, the slides should be protected from light from this step onwards.

l. Remove the secondary antibody.

m. Wash 3 times with 500–800 μL of 1× PBS per slide for 10 min/wash at room temperature (20°C–25°C).
n. Wash the slide once with 500–800 μL of distilled water per slide at room temperature (20°C–25°C) for 5 min.

20. Mount coverslips with Fluoromount G mounting media.
    a. Gently aspirate the distilled water from around the tissue, taking care not to aspirate the tissue.
    b. To avoid creating bubbles, dip a 500 μL pipet tip into Fluoromount G mounting media and add 4–5 drops of the medium on each slide by touching the pipet tip to the slide.
    c. Gently place the coverslip on the slide by hinging it from one end (Figure 3C).
    d. Allow Fluoromount G to solidify overnight or for 12–16 h in the dark at room temperature (20°C–25°C) before imaging.
    e. Seal the coverslips on the slides using a coverslip sealant.

EXPECTED OUTCOMES

In this protocol, cuprizone diet is fed to mice for 5 weeks, which results in acute demyelination (Figure 4A). Remyelination is observed as early as 2 weeks following cessation of cuprizone diet (Figures 4A and 4B), but complete remyelination may take about 6–10 weeks. The number of fate-mapped Gli1 cells labeled by RFP, NG2 positive oligodendrocyte progenitor cells, and CC1 positive mature oligodendrocytes, observed in the corpus callosum, are lower at peak demyelination i.e., 5 weeks of cuprizone diet, and gradually increase by 2 weeks following cessation of cuprizone diet (Figure 4B). EdU labeled proliferating cells do not show significant changes at these time points in the corpus callosum (Figure 4B). The proliferating cells in the corpus callosum are known to be a mix of oligodendrocyte progenitor cells, astrocytes and microglia.[5–7] Higher proliferation of cells following cuprizone diet, is also observed in the subventricular zone lining the lateral ventricles.[3,8] The late myelin proteins like MOG appear after 4 weeks of cuprizone withdrawal,[1] and myelinated segments of axons with mature nodes and paranodes are observed at 6–10 weeks following cessation of cuprizone diet.[3] Feeding the cuprizone diet for 12–15 weeks however, results in chronic demyelination with very little remyelination after withdrawal of cuprizone.[9,10]

LIMITATIONS

The extent of demyelination caused by cuprizone diet depends on the strain, age, and weight of the mice along with the cuprizone content and duration of the diet. 0.2% cuprizone diet produces demyelination in young adult mice of inbred strains like C57bl/6 but outbred strains like swiss webster mice need 0.4% cuprizone to produce similar levels of demyelination.[3,11] Mice older than 8 months age need higher cuprizone content in the diet to produce demyelination, compared to young adult mice of the same strain.[12–14] In addition, mice with low body weight at the start of cuprizone diet demyelinate to a greater extent than those with higher starting weights.[15] Finally, increasing the cuprizone content of the diet of young adult mice, from 0.2 to 0.5% increases the extent of demyelination with 0.5% cuprizone diet leading to status spongiosus in inbred strains, along with higher mortality.[16] In addition to mice, the cuprizone diet can be used to induce demyelination in rats[17,18] but it does not cause demyelination in non-human primates.[19]

Remarkably, different areas of the brain are demyelinated depending on the cuprizone content, duration, and strain of mice. Thus, in young adult C57bl/6 mice, 0.2% cuprizone diet for 5 weeks consistently produces complete demyelination of the corpus callosum, along with some demyelination in the cerebral cortex, basal ganglia, and cerebellar nuclei.[1,20–24] Within the corpus callosum, there are strain related differences with C57bl/6 mice showing more complete demyelination in the medial and caudal corpus callosum, CD1 mice exhibiting partial demyelination, and SJL/J mice showing extensive demyelination in the rostral and lateral areas of the callosum.[25–27] However, the spinal cord remains unaffected in both C57bl/6 and SJL/J mice.[28] In the cerebral cortex, 6 weeks of the diet causes complete demyelination in C57bl/6 mice, but partially affects the young adult

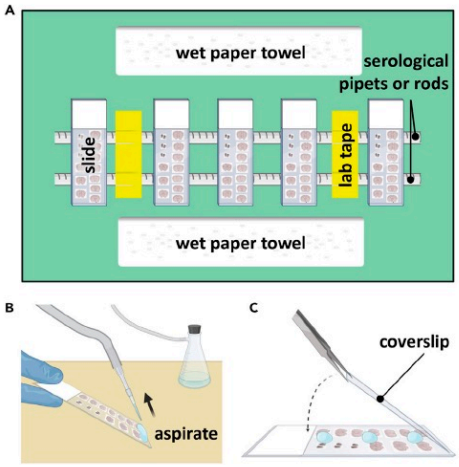

Figure 3. Immunolabeling of tissue sections
(A) Diagram of a humidity chamber for immunolabeling tissue slides.
(B) Tilting the slide for aspirating during washes, as well as using a 200 μL pipet tip on the end of the glass pipet attached to the suction tube to decrease the force of aspiration.
(C) Hinging the coverslip onto the slide during mounting.

BALB/cJ mice.[20] A 0.2% cuprizone diet for 7 weeks demyelinates the optic nerve[29] and for 6–12 weeks, results in demyelination of the hippocampus in C57bl/6 mice.[30–32] In the cerebellum, feeding 0.2% cuprizone diet for 12 weeks results in demyelination of the cortex and white matter in adult C57bl/6 mice,[33] while the superior cerebellar peduncle has been reported to be demyelinated when 0.5% cuprizone is fed to weanling mice of the outbred ICI strain.[34,35]

In the current protocol, we have reliably induced demyelination in the corpus callosum of young adult C57bl/6 mice by feeding 0.2% cuprizone diet for 5 weeks. Although we prefer to use pelleted diet, there are reports of the powdered diet being more potent at inducing demyelination, with the caveat that the control mice fed with powdered diet showed demyelination in one of the studies.[36–38] We switched to pelleted diet when the powdered diet significantly increased the mortality rate in both control and 0.2% cuprizone groups, after moving to a different facility. This was later found to be due to a change in the air circulation within the cages in the new facility, which increased the inhalation of powdered diet causing inflammation in the lungs. Hence, powdered diet should be used with caution.

TROUBLESHOOTING

Problem 1

The liver does not appear pale and the body and tail are relaxed after perfusion.

The perfusate did not flow through the systemic circulation (step 7).

Potential solution

The tip of the butterfly needle may have pierced through the interventricular septum into the right ventricle, and the perfusate may be flowing into the right ventricle. Gently pull out the needle and reposition it until the tip is in the left ventricle. The brain can be perfused well even if the perfusate flows partially through the systemic circulation i.e., from the left ventricle to the aorta.

CellPress
OPEN ACCESS

STAR Protocols
Protocol

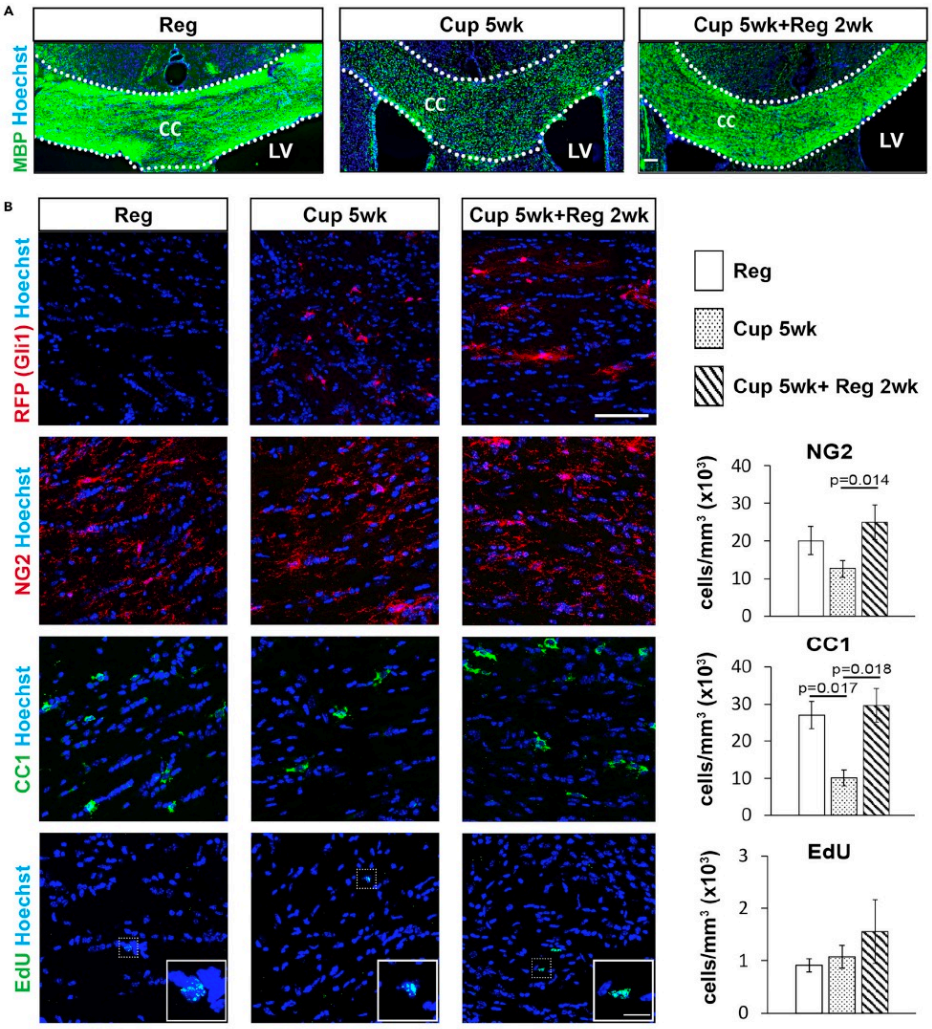

Figure 4. Immunofluorescence and EdU labeling

(A) Immunofluorescent labeling of brain cryosections from mice fed with regular diet (Reg), 0.2% cuprizone diet for 5 weeks (Cup 5wk), and 0.2% cuprizone diet for 5 weeks followed by two weeks regular diet (Cup 5wk + Reg 2wk), showing MBP in the corpus callosum (CC) outlined with white dotted lines. Scale bars = 50 μm, Subventricular zone (SVZ), Lateral ventricle (LV).

(B) Examples of immunofluorescent labeling of CC1 expressing mature oligodendrocytes, NG2 expressing oligodendrocyte precursor cells, RFP expressing Gli1 fate mapped cells, and EdU positive proliferating cells in the CC of mice fed with regular diet, cuprizone diet for 5 weeks, and cuprizone diet for 5 weeks followed by two weeks regular diet, with quantification of CC1, NG2, and EdU positive cells in the corpus callosum. N = 3, Data = Mean ± SEM, One-way ANOVA with Tukey's post-hoc t-test, Scale bars = 25 μm, inset scale bar = 5 μm.

Problem 2
Lungs inflate and/or fluid leaks through the mouth and nose during perfusion.

The perfusate is flowing through the pulmonary circulation (step 7).

Potential solution
If the entire perfusate flows through the right ventricle into the pulmonary arteries, the lungs inflate and the bronchial capillaries rupture leading to leakage of frothy fluid from the mouth and nose. Gently pull out the needle and reposition it until the tip is in the left ventricle. The brain can be perfused well even if the perfusate flows partially through the systemic circulation.

Problem 3
The olfactory bulbs are missing from the harvested brain.

Olfactory bulbs tear away when the brain is removed from the skull (step 8).

Potential solution
To prevent the olfactory bulbs from tearing off, ensure that they are no longer attached to the bone before attempting to remove the brain. Removing the bone around the olfactory bulbs may require some extra trimming of the bone with a small pair of scissors. Carefully cut the bone between the two bulbs to release them, as well as gently nudge them away from the bone by the closed tips of fine forceps.

Problem 4
Tearing of tissue during cryosectioning.

The brain is soft and the sections break apart while collecting them on the slide (step 14).

Potential solution
This is most often a result of incomplete perfusion especially if the brain looks bloody or pink after harvesting. During perfusion, ensure that the butterfly needle tip is fully inserted into the left ventricle and the perfusate flows through the systemic circulation. Shattering of tissue is also seen when either the brain or the cryostat temperature is too cold. Keeping the brain in the cryostat long enough to equilibrate its temperature with that of the cryostat and/or increasing the cryostat temperature by 1°C–2°C can make the sectioning smoother.

Problem 5
Stripes of torn tissue in the sections.

The sections show thin stripes perpendicular to the edge of the blade or thick stripes of irregular shape (step 14).

Potential solution
Nicks on the blade can result in thin stripes perpendicular to the edge. Move the blade or the stage to section the brain with an unused edge of the blade. When either tissue or OCT adheres to the edge of the blade, it can result in thicker stripes and sudden difficulty in cryosectioning. Clean the blade by wiping with the gauze sponge in perpendicular strokes away from the edge of the blade, taking care to avoid cutting your fingers.

Problem 6
No sections on the slide after immunofluorescence.

Tissue lifts off the slide and floats away during immunofluorescent labeling (step 19).

CellPress
OPEN ACCESS

STAR Protocols
Protocol

Potential solution

If the tissue section is not in direct contact with the glass slide, then the sections do not adhere to the slide during the immunofluorescent wash steps. This is often due to presence of a layer of OCT between the tissue and the glass surface. To prevent this situation, make sure you wipe off the OCT or unwanted sections from the slide with a gauze sponge dipped in PBS or water and dry the surface before collecting a section on the same surface, during cryosectioning.

RESOURCE AVAILABILITY

Lead contact

Further information and requests for resources and reagents should be directed to and will be fulfilled by the lead contact, Jayshree Samanta (jayshree.samanta@wisc.edu).

Materials availability

No materials were newly generated in this course of this study.

Data and code availability

Not applicable.

ACKNOWLEDGMENTS

This article was funded by the University of Wisconsin-Madison Stem Cell and Regenerative Medicine Center Postdoctoral Fellowship (D.Z.R.), NIH/NINDS grants R01NS119517 (J.S.) and R03NS126993 (J.S.), the Boespflug Myopathic Research Foundation (J.S.), and the University of Wisconsin-Madison Office of the Vice Chancellor for Research and Graduate Education with funding from the Wisconsin Alumni Research Foundation (J.S.). Figures were created with BioRender.

AUTHOR CONTRIBUTIONS

E.C.D. performed experiments using this protocol, fine-tuned the protocol, and wrote the manuscript. D.Z.R. performed experiments using this protocol, fine-tuned the protocol, and edited the manuscript. J.S. developed the original protocol, supervised the experiments, and edited the manuscript.

DECLARATION OF INTERESTS

J.S. is a co-inventor in the patent US 9,248,128 and a consultant for GliXogen Therapeutics.

REFERENCES

1. Radecki, D.Z., Messling, H.M., Haggerty-Skeans, J.R., Bhamidipati, S.K., Clawson, E.D., Overman, C.A., Thatcher, M.M., Salzer, J.L., and Samanta, J. (2020). Relative levels of Gli1 and Gli2 determine the response of ventral neural stem cells to demyelination. Stem Cell Rep. *15*, 1047–1055. https://doi.org/10.1016/j.stemcr.2020.10.003.

2. Schindelin, J., Arganda-Carreras, I., Frise, E., Kaynig, V., Longair, M., Pietzsch, T., Preibisch, S., Rueden, C., Saalfeld, S., Schmid, B., et al. (2012). Fiji: an open-source platform for biological-image analysis. Nat. Methods *9*, 676–682. https://doi.org/10.1038/nmeth.2019.

3. Samanta, J., Grund, E.M., Silva, H.M., Lafaille, J.J., Fishell, G., and Salzer, J.L. (2015). Inhibition of Gli1 mobilizes endogenous neural stem cells for remyelination. Nature *526*, 448–452. https://doi.org/10.1038/nature14957.

4. Samanta, J., Silva, H.M., Lafaille, J.J., and Salzer, J.L. (2021). Transcriptomic analysis of loss of Gli1 in neural stem cells responding to demyelination in the mouse brain. Sci. Data *8*, 278. https://doi.org/10.1038/s41597-021-01063-x.

5. Remington, L.T., Babcock, A.A., Zehntner, S.P., and Owens, T. (2007). Microglial recruitment, activation, and proliferation in response to primary demyelination. Am. J. Pathol. *170*, 1713–1724. https://doi.org/10.2353/ajpath.2007.060783.

6. Hibbits, N., Yoshino, J., Le, T.Q., and Armstrong, R.C. (2012). Astrogliosis during acute and chronic cuprizone demyelination and implications for remyelination. ASN Neuro *4*, 393–408. https://doi.org/10.1042/AN20120062.

7. Hillis, J.M., Davies, J., Mundim, M.V., Al-Dalahmah, O., and Szele, F.G. (2016). Cuprizone demyelination induces a unique inflammatory response in the subventricular zone. J. Neuroinflamm. *13*, 190. https://doi.org/10.1186/s12974-016-0651-2.

8. Silvestroff, L., Bartucci, S., Soto, E., Gallo, V., Pasquini, J., and Franco, P. (2010). Cuprizone-induced demyelination in CNP::GFP transgenic mice. J. Comp. Neurol. *518*, 2261–2283. https://doi.org/10.1002/cne.22330.

9. Mason, J.L., Toews, A., Hostettler, J.D., Morell, P., Suzuki, K., Goldman, J.E., and Matsushima, G.K. (2004). Oligodendrocytes and progenitors become progressively depleted within chronically demyelinated lesions. Am. J. Pathol. *164*, 1673–1682. https://doi.org/10.1016/S0002-9440(10)63726-1.

10. Matsushima, G.K., and Morell, P. (2001). The neurotoxicant, cuprizone, as a model to study demyelination and remyelination in the central nervous system. Brain Pathol. *11*, 107–116. https://doi.org/10.1111/j.1750-3639.2001.tb00385.x.

11. Elsworth, S., and Howell, J.M. (1973). Variation in the response of mice to cuprizone. Res. Vet. Sci. *14*, 385–387.

12. Shen, S., Sandoval, J., Swiss, V.A., Li, J., Dupree, J., Franklin, R.J.M., and Casaccia-Bonnefil, P. (2008). Age-dependent epigenetic control of differentiation inhibitors is critical for remyelination efficiency. Nat. Neurosci. *11*, 1024–1034. https://doi.org/10.1038/nn.2172.

13. Irvine, K.A., and Blakemore, W.F. (2006). Age increases axon loss associated with primary demyelination in cuprizone-induced demyelination in C57BL/6 mice. J. Neuroimmunol. *175*, 69–76. https://doi.org/10.1016/j.jneuroim.2006.03.002.

14. Gingele, S., Henkel, F., Heckers, S., Moellenkamp, T.M., Hummert, M.W., Skripuletz, T., Stangel, M., and Gudi, V. (2020). Delayed demyelination and impaired remyelination in aged mice in the cuprizone model. Cells *9*. https://doi.org/10.3390/cells9040945.

15. Leopold, P., Schmitz, C., and Kipp, M. (2019). Animal weight is an important variable for reliable cuprizone-induced demyelination. J. Mol. Neurosci. *68*, 522–528. https://doi.org/10.1007/s12031-019-01312-0.

16. Suzuki, K., and Kikkawa, Y. (1969). Status spongiosus of CNS and hepatic changes induced by cuprizone (biscyclohexanone oxalyldihydrazone). Am. J. Pathol. *54*, 307–325.

17. Love, S. (1988). Cuprizone neurotoxicity in the rat: morphologic observations. J. Neurol. Sci. *84*, 223–237. https://doi.org/10.1016/0022-510x(88)90127-x.

18. Basoglu, H., Boylu, N.T., and Kose, H. (2013). Cuprizone-induced demyelination in Wistar rats; electrophysiological and histological assessment. Eur. Rev. Med. Pharmacol. Sci. *17*, 2711–2717.

19. Chen, Z., Chen, J.T., Johnson, M., Gossman, Z.C., Hendrickson, M., Sakaie, K., Martinez-Rubio, C., Gale, J.T., and Trapp, B.D. (2015). Cuprizone does not induce CNS demyelination in nonhuman primates. Ann. Clin. Transl. Neurol. *2*, 208–213. https://doi.org/10.1002/acn3.159.

20. Skripuletz, T., Lindner, M., Kotsiari, A., Garde, N., Fokuhl, J., Linsmeier, F., Trebst, C., and Stangel, M. (2008). Cortical demyelination is prominent in the murine cuprizone model and is strain-dependent. Am. J. Pathol. *172*, 1053–1061. https://doi.org/10.2353/ajpath.2008.070850.

21. Groebe, A., Clarner, T., Baumgartner, W., Dang, J., Beyer, C., and Kipp, M. (2009). Cuprizone treatment induces distinct demyelination, astrocytosis, and microglia cell invasion or proliferation in the mouse cerebellum. Cerebellum *8*, 163–174. https://doi.org/10.1007/s12311-009-0099-3.

22. Gudi, V., Moharregh-Khiabani, D., Skripuletz, T., Koutsoudaki, P.N., Kotsiari, A., Skuljec, J., Trebst, C., and Stangel, M. (2009). Regional differences between grey and white matter in cuprizone induced demyelination. Brain Res. *1283*, 127–138. https://doi.org/10.1016/j.brainres.2009.06.005.

23. Pott, F., Gingele, S., Clarner, T., Dang, J., Baumgartner, W., Beyer, C., and Kipp, M. (2009). Cuprizone effect on myelination, astrogliosis and microglia attraction in the mouse basal ganglia. Brain Res. *1305*, 137–149. https://doi.org/10.1016/j.brainres.2009.09.084.

24. Goldberg, J., Clarner, T., Beyer, C., and Kipp, M. (2015). Anatomical distribution of cuprizone-induced lesions in C57BL6 mice. J. Mol. Neurosci. *57*, 166–175. https://doi.org/10.1007/s12031-015-0595-5.

25. Taylor, L.C., Gilmore, W., and Matsushima, G.K. (2009). SJL mice exposed to cuprizone intoxication reveal strain and gender pattern differences in demyelination. Brain Pathol. *19*, 467–479. https://doi.org/10.1111/j.1750-3639.2008.00230.x.

26. Steelman, A.J., Thompson, J.P., and Li, J. (2012). Demyelination and remyelination in anatomically distinct regions of the corpus callosum following cuprizone intoxication. Neurosci. Res. *72*, 32–42. https://doi.org/10.1016/j.neures.2011.10.002.

27. Yu, Q., Hui, R., Park, J., Huang, Y., Kusnecov, A.W., Dreyfus, C.F., and Zhou, R. (2017). Strain differences in cuprizone induced demyelination. Cell Biosci. *7*, 59. https://doi.org/10.1186/s13578-017-0181-3.

28. Herder, V., Hansmann, F., Stangel, M., Skripuletz, T., Baumgärtner, W., and Beineke, A. (2011). Lack of cuprizone-induced demyelination in the murine spinal cord despite oligodendroglial alterations substantiates the concept of site-specific susceptibilities of the central nervous system. Neuropathol. Appl. Neurobiol. *37*, 676–684. https://doi.org/10.1111/j.1365-2990.2011.01168.x.

29. Marenna, S., Huang, S.C., Dalla Costa, G., d'Isa, R., Castoldi, V., Rossi, E., Comi, G., and Leocani, L. (2022). Visual evoked potentials to monitor myelin cuprizone-induced functional changes. Front. Neurosci. *16*, 820155. https://doi.org/10.3389/fnins.2022.820155.

30. Hoffmann, K., Lindner, M., Gröticke, I., Stangel, M., and Löscher, W. (2008). Epileptic seizures and hippocampal damage after cuprizone-induced demyelination in C57BL/6 mice. Exp. Neurol. *210*, 308–321. https://doi.org/10.1016/j.expneurol.2007.11.005.

31. Koutsoudaki, P.N., Skripuletz, T., Gudi, V., Moharregh-Khiabani, D., Hildebrandt, H., Trebst, C., and Stangel, M. (2009). Demyelination of the hippocampus is prominent in the cuprizone model. Neurosci. Lett. *451*, 83–88. https://doi.org/10.1016/j.neulet.2008.11.058.

32. Norkute, A., Hieble, A., Braun, A., Johann, S., Clarner, T., Baumgartner, W., Beyer, C., and Kipp, M. (2009). Cuprizone treatment induces demyelination and astrocytosis in the mouse hippocampus. J. Neurosci. Res. *87*, 1343–1355. https://doi.org/10.1002/jnr.21946.

33. Skripuletz, T., Bussmann, J.H., Gudi, V., Koutsoudaki, P.N., Pul, R., Moharregh-Khiabani, D., Lindner, M., and Stangel, M. (2010). Cerebellar cortical demyelination in the murine cuprizone model. Brain Pathol. *20*, 301–312. https://doi.org/10.1111/j.1750-3639.2009.00271.x.

34. Blakemore, W.F. (1973). Demyelination of the superior cerebellar peduncle in the mouse induced by cuprizone. J. Neurol. Sci. *20*, 63–72. https://doi.org/10.1016/0022-510x(73)90118-4.

35. Blakemore, W.F. (1973). Remyelination of the superior cerebellar peduncle in the mouse following demyelination induced by feeding cuprizone. J. Neurol. Sci. *20*, 73–83. https://doi.org/10.1016/0022-510x(73)90119-6.

36. Hagemeyer, N., Boretius, S., Ott, C., Von Streitberg, A., Welpinghus, H., Sperling, S., Frahm, J., Simons, M., Ghezzi, P., and Ehrenreich, H. (2012). Erythropoietin attenuates neurological and histological consequences of toxic demyelination in mice. Mol. Med. *18*, 628–635. https://doi.org/10.2119/molmed.2011.00457.

37. Hochstrasser, T., Exner, G.L., Nyamoya, S., Schmitz, C., and Kipp, M. (2017). Cuprizone-containing pellets are less potent to induce consistent demyelination in the corpus callosum of C57BL/6 mice. J. Mol. Neurosci. *61*, 617–624. https://doi.org/10.1007/s12031-017-0903-3.

38. Toomey, L.M., Papini, M., Lins, B., Wright, A.J., Warnock, A., McGonigle, T., Hellewell, S.C., Bartlett, C.A., Anyaegbu, C., and Fitzgerald, M. (2021). Cuprizone feed formulation influences the extent of demyelinating disease pathology. Sci. Rep. *11*, 22594. https://doi.org/10.1038/s41598-021-01963-3.